

Article

Middle Silurian–Middle Devonian Magmatic Rocks in the Eastern Segment of the Northern Margin of the North China Craton: Implications for Regional Tectonics

Bin Li ^{1,2}, Jingsheng Chen ^{1,2,*}, Fan Yang ³, Miao Liu ^{1,2}, Yanqing Zang ^{1,2} and Chao Zhang ^{1,2}

¹ Shenyang Geological Survey Center of China Geological Survey, Shenyang 110034, China; libin@mail.cgs.gov.cn

² Northeast Geological S&T Innovation Center of China Geological Survey, Shenyang 110034, China

³ College of Resources and Environment, Jilin Agricultural University, Changchun 130061, China

* Correspondence: chenjingsheng@mail.cgs.gov.cn

Abstract: This paper presents a detailed study including LA-ICP-MS zircon U-Pb dating, geochemical, zircon Hf isotope, and whole rock Sr-Nd isotope analysis of magmatic rocks from the Yitong County, Jilin Province, NE China. These data are used to better constrain the Middle Silurian–Middle Devonian tectonic evolution in the eastern segment of the northern margin of the North China Craton (NCC). Zircon U-Pb dating results show that the Ximangzhang tonalite formed in the Late Silurian (425 ± 6 Ma); the basalt, andesite, and metamorphic olivine-bearing basalt in the Fangniugou volcanic rocks formed in the Middle Silurian (428 ± 6.6 Ma) and Middle Devonian (388.4 ± 3.9 Ma, and 384.1 ± 4.9 Ma). The Late Silurian tonalites are characterized by high SiO_2 and Na_2O and low K_2O , MgO , FeOT , and TiO_2 , with an A/CNK ratio of 0.91–1.00, characteristic of calc-alkaline I-type granite. They are enriched in Rb, Ba, Th, U, and K, and depleted in Nb, Sr, P, and Ti, with positive $\epsilon_{\text{Nd}}(t)$ (+0.35) and $\epsilon_{\text{Hf}}(t)$ (+0.44 to +6.31) values, suggesting that they mainly originated from the partial melting of Meso–Neoproterozoic accretionary lower crustal material (basalt). The Middle Silurian basalts are characterized by low SiO_2 , P_2O_5 , TiO_2 , and Na_2O and high Al_2O_3 , FeOT , and K_2O , enriched in Rb, Ba, Th, U, and K and depleted in Nb, Ta, Sr, P, and Ti, indicative of shoshonitic basalt. The Late Silurian tonalites have positive $\epsilon_{\text{Nd}}(t)$ (+4.91 to +6.18) values and primarily originated from depleted mantle magmas metasomatized by subduction fluids, supplemented by a small amount of subducted sediments and crustal materials. The Middle Devonian volcanic rocks exhibit low SiO_2 , TiO_2 , and Na_2O and high K_2O , and MgO , enriched in Rb, K, and LREEs and depleted in Nb, Ta, Sr, and HREEs, characteristic of shoshonitic volcanic rocks. Their $\epsilon_{\text{Nd}}(t)$ (+2.11 to +3.77) and $\epsilon_{\text{Hf}}(t)$ (+5.90 to +11.73) values are positive. These characteristics indicate that the Middle Devonian volcanic rocks primarily originated from depleted mantle magmas metasomatized by subduction fluids, with the addition of crustal materials or subducted sediments during their formation. Based on regional geological data, it is believed that the study area underwent the following evolutionary stages during the Silurian–Devonian period: (1) active continental margin stage of southward subduction of the Paleo–Asian Ocean (PAO) (443–419 Ma); (2) arc-continent collision stage (419–405 Ma); (3) post-collision extension stage (404–375 Ma); (4) active continental margin stage, with the PAO plate subducting southward once again (375–360 Ma).

Keywords: Silurian; Devonian; magmatic rocks; geochronology; geochemistry; petrogenesis; the eastern segment of the northern margin of the North China Craton



Citation: Li, B.; Chen, J.; Yang, F.; Liu, M.; Zang, Y.; Zhang, C. Middle Silurian–Middle Devonian Magmatic Rocks in the Eastern Segment of the Northern Margin of the North China Craton: Implications for Regional Tectonics. *Minerals* **2024**, *14*, 641. <https://doi.org/10.3390/min14070641>

Academic Editor: Alexandre V. Andronikov

Received: 19 May 2024

Revised: 15 June 2024

Accepted: 17 June 2024

Published: 23 June 2024



Copyright: © 2024 by the authors. Licensee MDPI, Basel, Switzerland. This article is an open access article distributed under the terms and conditions of the Creative Commons Attribution (CC BY) license (<https://creativecommons.org/licenses/by/4.0/>).

1. Introduction

The Central Asian Orogenic Belt (CAOB), situated between the North China, Tarim, and Siberian plates [1–6], represents the largest accretionary orogenic belt of the Phanerozoic. The CAOB is noted for its extensive crustal growth and significant mineralization

potential during the same period [7–10]. The formation of the CAOB involved the subduction of the Paleo–Asian Ocean (PAO) and the amalgamation of terranes, consisting of a series of microcontinents, island arcs, accretionary complexes, ophiolites, forearc/back-arc basins, oceanic plateaus, and seamounts [1,4,11]. With a highly complicated geological tectonic evolution [12], the CAOB serves as a critical area for studying the processes of collision and amalgamation of micro-continents, continental accretion, and ocean-continent transitions [6,13–17]. There is a consensus among scholars that the PAO closed along the Solonker-Xar Moron-Changchun-Yanji Suture (SXCYS) on the southeastern margin of the CAOB (Figure 1a) [4,6,12,13,18–29].

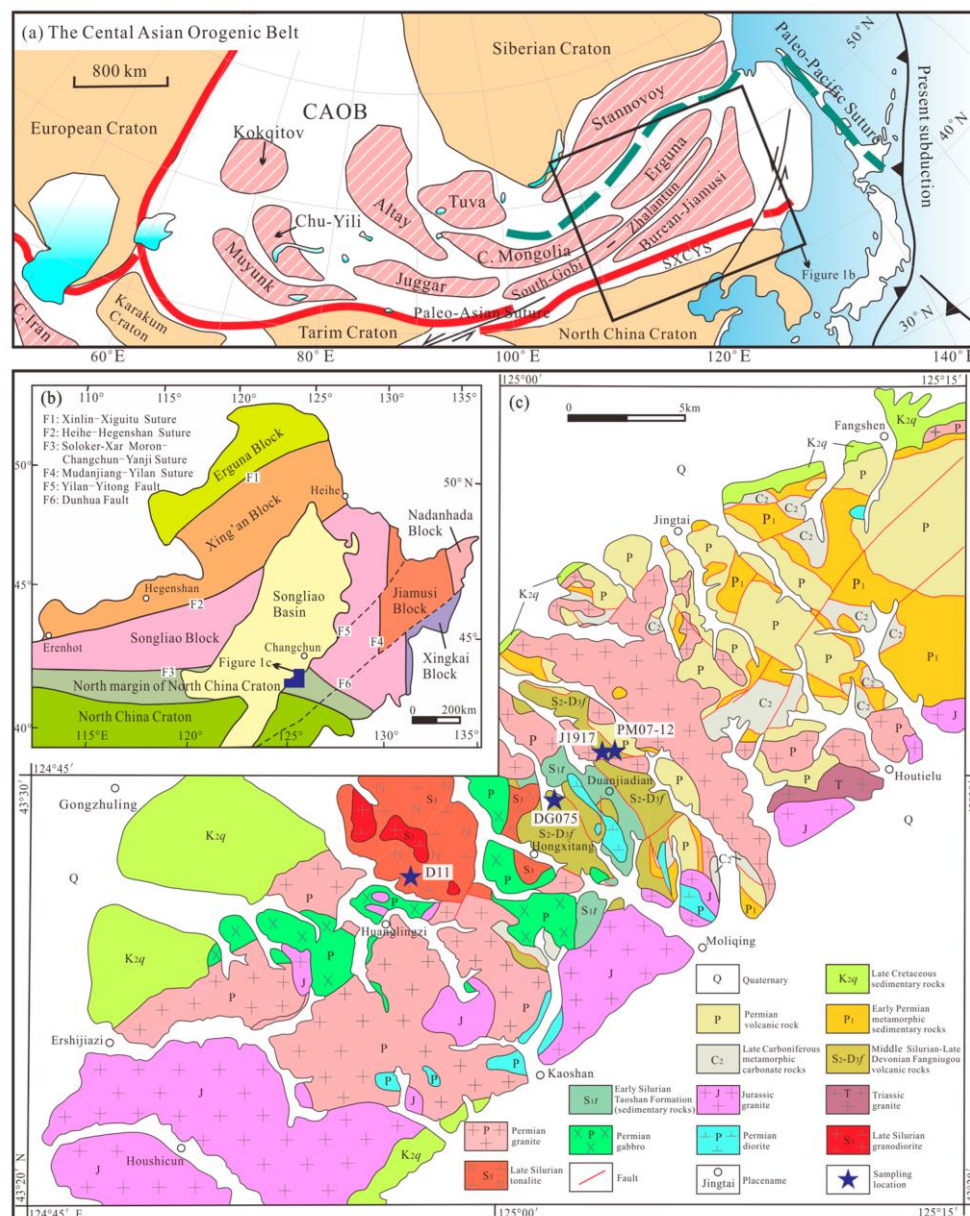


Figure 1. (a) Tectonic division of the Central Asian Orogenic Belt and adjacent regions (modified after [22]), and the position of Figure 1b (black color square); (b) Tectonic division of NE China (modified from [12]); (c) Geological sketch map of the Yitong area in Jilin Province (modified from [29]).

The northern margin of the North China Craton (NCC) is located at the southeastern margin of the CAOB (Figure 1a,b), north of the Bayan Obo–Chifeng–Kaiyuan fault and south of the SXCYS. This area primarily encompasses the Bainaimiao arc and the Ondor Sum subduction–accretionary complex [20,30,31]. The Bainaimiao arc extends approximately

1300 km from Baoerhantu to Bayan Obo, Bainaimiao, and Chifeng in Inner Mongolia to eastern Faku in Liaoning Province to northeastern Gongzhuling and Yanbian in Jilin Province [32]. At present, there are still different opinions on the basement properties, subduction polarity, and tectonic setting of the Bainaimiao arc. One suggests affinity of the arc basement with the NCC and the other proposes affinity with other continental blocks. It is also suggested that the Bainaimiao arc belt and the Ondor Sum subduction-accretionary complex constitute a trench-arc-basin system formed by the southward subduction of the PAO [15,20,33–41]; however, some argue for its formation through the northward subduction of the South Bainaimiao Ocean, accreting to the NCC via arc-continent collision [32,42–48]. Consequently, the Bainaimiao arc belt has been regarded as a Japan-style island arc [37,49,50], Andean-type continental margin arc [20,51], or exotic terrain [42]. In addition, there is controversy about the formation age of the Bainaimiao arc, suggested to be Middle Neoproterozoic [50,52,53] or Ordovician–Silurian [32,51,54,55].

Previous research was predominantly focused on the central and western regions of Inner Mongolia, while the northern margin of the NCC from northern Liaoning Province to central Jilin Province has received less attention [32,43,45,56,57]. Moreover, the northern Liaoning Province to central Jilin Province region, which was originally classified as Early Paleozoic, has now been classified as Late Paleozoic or Early Mesozoic [12,19,51,58–66]. Therefore, it remains uncertain whether the Bainaimiao arc belt can extend over the Songliao Basin into northeastern China [12,58,59,67]. With the deepening of research, some Ordovician–Devonian rocks have been discovered in recent years in northern Liaoning Province and central to eastern Jilin Province [43,44,48,56,64,68–71], providing valuable information for further understanding of tectonic evolution. The Silurian–Devonian rocks in Yitong County, Jilin Province, which document a continuous evolutionary history from the Silurian to the Permian, are particularly crucial for exploring the tectonic framework and accretionary processes along the eastern segment of the northern margin of the NCC. In this study, zircon U–Pb chronological, petrographical, geochemical, zircon Hf-isotope, and whole-rock Sr–Nd isotope analyses were conducted (Table 1), and the properties and tectonic setting of the source area of the Silurian–Devonian magmatic rocks in Yitong area are discussed. These data provide new evidence for the magmatic-tectonic evolution of the northern margin of the NCC in the Silurian–Devonian.

Table 1. The simplified list of the volcanic and intrusive rock samples in this study.

Age	Lithology	GPS	Samples No.
425 ± 6 Ma	Tonalite	E124°56′07″, N43°27′42″	Zircon U–Pb and Hf Isotope: D11 Whole-Rock: D11-1-1, D11-1-2, D11-1-3, D11-1-4 Sr–Nd: D11-1-1 Zircon U–Pb: DG075
428 ± 6.6 Ma	Basalt	E125°01′31″, N43°29′37″	Whole-Rock: DG075-1, DG075-2, DG075-3, DG075-4 Sr–Nd: DG075-1, DG075-2 Zircon U–Pb and Hf Isotope: J1917
388.4 ± 3.9 Ma	Andesite	E125°03′24″, N43°30′29″	Whole-Rock: J1917-2, J1917-5 Sr–Nd: J1917-2, J1917-5 Zircon U–Pb: PM07-12
384.1 ± 4.9 Ma	Metamorphic olivine-bearing basalt	E125°04′12″, N43°30′28″	Whole-Rock: PM07-9-2, PM07-9-4, PM07-9-5

2. Geological Setting and Samples

2.1. Geological Setting

The study area is located in the northwest of Yitong County, Jilin Province, Northeast China (Figure 1c). It is adjacent to the Yitong Basin to the east and the Songliao Basin to the west, belonging to the southeast margin of the CAOB and the eastern margin of the

NCC. This area mainly contains the Lower Silurian Taoshan Formation, Upper Silurian–Upper Devonian Fangniugou volcanic rocks, Upper Carboniferous metamorphic carbonate rocks, Lower Permian metamorphic clastic rocks, and Permian volcanic rocks. The main lithology of the Taoshan Formation consists of sandstone, siltstone, silty mudstone, and silty slate, interbedded with marlstone, and contains gracilite. Intrusive rocks include the Late Ordovician–Late Silurian tonalite and granodiorite; Middle–Late Permian granodiorite, monzonite, quartz monzonite, and gabbro; Early Triassic monzogranite; and Early–Middle Jurassic syenite granite, granodiorite, monzogranite and quartz diorite.

Fangniugou volcanic rocks, established as an informal mapping unit [72], primarily consist of intermediate to acidic volcanic rocks considered to have formed during the Ordovician. In recent years, scholars have obtained zircon U–Pb ages of 426 ± 4.8 Ma [29], 402 ± 4 Ma [68], 419 ± 3 Ma [43], 425 ± 4 Ma, 390 ± 4 Ma [44], and 375.5 ± 4.6 Ma [29] from the Fangniugou volcanic rocks, suggesting that they were formed during the Late Silurian to Late Devonian period.

In the northeast of the Taoshan Formation, the Fangniugou volcanic rocks are exposed with a suite of metamorphic carbonates, clastic rocks, and volcanic rocks, which formed during the Carboniferous to Permian [32,45] (Figure 1c). The Paleozoic geological units in the study area are composed of a series of tectonic slices, which were formed during the Silurian to Permian, and gradually became younger from southwest to northeast. Reflected in the process of oceanic crust subduction, various geological bodies of different ages and environments were, in turn, collaged laterally, and then transformed by later tectonic events.

2.2. Sample Descriptions

The tonalite (D11) is gray in color, with a mylonitic structure and a fine-grained granitic texture (Figure 2a,b). The sample shows a typical mineral assemblage of plagioclase (~55 vol.%), quartz (~25 vol.%), biotite (~20 vol.%), and minor accessory minerals (~5 vol.%; e.g., allanite, epidote).

The basalt (DG075) is dark gray in color and shows a porphyritic texture with 27% phenocrysts (Figure 2c,d). The phenocrysts are mainly alkali feldspar (15%) and hornblende (12%). The matrix (73%) is predominantly microcrystalline and includes hornblende, alkali feldspar, and plagioclase.

The andesite (J1917) is gray in color and shows a porphyritic texture with 8% phenocrysts (Figure 2e,f). The phenocrysts are composed of plagioclase (5%) and hornblende (3%). Plagioclase undergoes alteration such as sericitization and chloritization. The matrix (92%) is predominantly microcrystalline and includes biotite, chlorite, sericite, felsic minerals, etc.

The metamorphic olivine-bearing basalt (PM07-12) is greenish–gray in color, with a porphyroblastic texture and massive structure (Figure 2g,h). The porphyroblasts are zoisite (6%), garnet (3%), and olivine (3%). The matrix (88%) is predominantly microcrystalline and includes zoisite, sericite, and plagioclase.

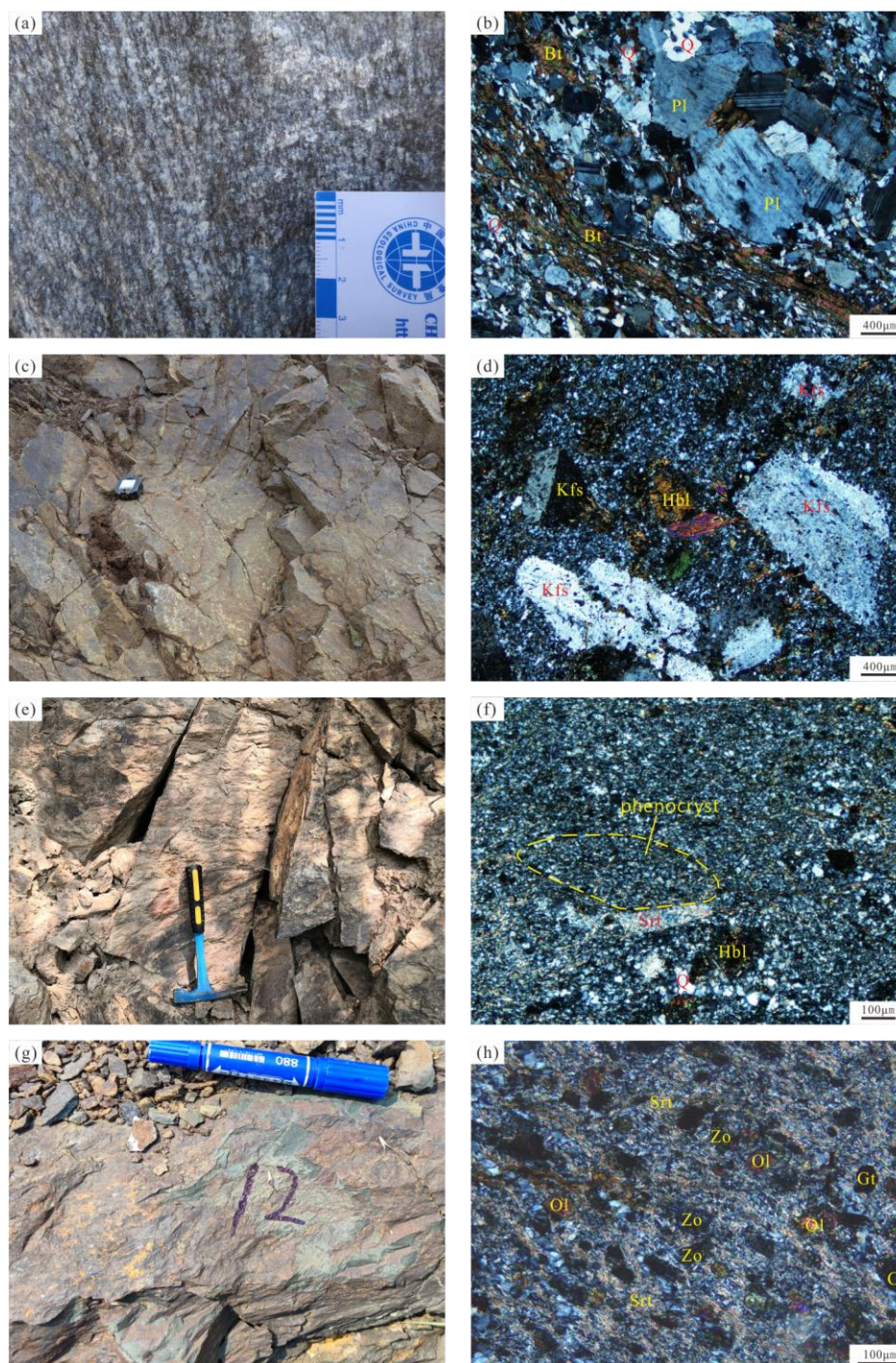


Figure 2. Field photographs and microphotographs of the Middle Silurian–Middle Devonian magmatic rocks from the Yitong area. (a,b) Tonalite (Sample D11); (c,d) Basalt (Sample DG075); (e,f) Andesite (Sample J1917); (g,h) Metamorphic olivine-bearing basalt (Sample PM07-12. In the figure, 12 represents the layer number of profile 07). Abbreviations: Qz, Quartz; Pl, Plagioclase; Kfs, K-feldspar; Srt, Sericite; Bi, Biotite; Hbl, hornblende; Ol, olivine; Ep, epidote; Zo, Zoisite; Grt, Garnet.

3. Analytical Methods

3.1. Whole-Rock Composition Analyses

Geochemical analyses of the rock samples were conducted at the Northeast China Supervision Inspection Center of Mineral Resources, Ministry of Natural Resources, Shenyang Center of Geological Survey, China Geological Survey, Shenyang, China, using

contamination-free equipment. Major elements were quantified via X-ray fluorescence spectrometry (XRF), with errors in precision and accuracy of $\pm 5\%$. Trace elements were measured using Inductively Coupled Plasma Mass Spectrometry (ICP-MS), with errors in precision and accuracy of less than 10%.

3.2. LA-ICP-MS Zircon U-Pb Dating

LA-ICP-MS Zircon U-Pb dating was performed at the Key Laboratory of Mineral Resources Evaluation in Northeast Asia, Ministry of Natural Resources, Jilin University, Changchun, China. The process utilized a COMPEX Pro type ArF excimer laser ablation system from the Coherent Company (Saxonburg, PA, USA) and an Agilent 7900 type ICP-MS (Agilent Technologies, Inc., Santa Clara, CA, USA). The laser spot diameter was set at 32 μm . High-purity helium served as the carrier gas, and argon was used as the auxiliary gas. Isotopic ratio corrections employed standard zircons 91500 and PLE, while the international standard NIST610 corrected the contents of Th, U, Pb, and other elements [73]. The procedures followed for these analyses are elaborated in Yuan et al. [74]. Age determinations were conducted using Isoplot software (version 3.0).

3.3. Zircon Lu-Hf Isotopic Analyses

Zircon Lu-Hf isotopic analyses were carried out at the Tianjin Institute of Geology and Mineral Resources. This process utilized a Thermo Fisher Neptune type Multi-Collector Inductively Coupled Plasma Mass Spectrometer (MC-ICPMS) and a 193 nm laser ablation system (NEW WAVE193nm FX), with a laser spot size of 50 μm (Thermo Fisher Scientific, Waltham, MA, USA). The methodologies applied, including isotopic fractionation corrections, are based on the techniques described by Geng Jianzhen et al. [75] and Wu Fuyuan et al. [17].

3.4. Whole-Rock Sr-Nd Isotopic Analyses

Whole-rock Sr-Nd isotopic analyses were conducted at the Analytical and Testing Research Center of the Beijing Research Institute of Uranium Geology. These analyses utilized an ISOPROBE-T thermal ionization mass spectrometer (Isotopx LTD., Cheshire, UK). The isotopic ratios for Sr and Nd were standardized using the values $^{86}\text{Sr}/^{88}\text{Sr} = 0.1194$ and $^{146}\text{Nd}/^{144}\text{Nd} = 0.7219$.

4. Analysis Results

4.1. Zircon U-Pb Geochronology

The zircon U-Pb dating results are shown in Supplementary Table S1.

Sample D11 is a tonalite from the Ximangzhang pluton. Twenty-five zircon grains from this sample were dated, with most results lying on or near the concordia line. These zircons are mostly granular and short columnar, with grain sizes of 100–200 μm and length/width ratios of 1:1 to 3:2. The cathodoluminescence (CL) images (Figure 3a) show that these zircon grains have typical zonal textures and Th/U ratios of 0.36–0.77, suggesting a magmatic origin. Of these, 17 zircon grains have $^{206}\text{Pb}/^{238}\text{U}$ ages of 420–437 Ma, with a weighted mean $^{206}\text{Pb}/^{238}\text{U}$ age of 425 ± 6 Ma (mean squared weighted deviation (MSWD) = 0.12) (Figure 4a), representing the best estimate for emplacement time of the tonalite. Another 8 zircon grains have $^{206}\text{Pb}/^{238}\text{U}$ ages of 445–459 Ma, with a weighted mean $^{206}\text{Pb}/^{238}\text{U}$ age of 451 ± 10 Ma (MSWD = 0.08).

Sample DG075 is a basalt from the Fangniugou volcanic rocks. These zircons are short columnar, with grain sizes of 50–100 μm and length/width ratios of 2:1 to 3:2. The CL images (Figure 3b) show that these zircon grains have typical zonal textures and Th/U ratios of 0.41–0.75, suggesting magmatic zircons. Twenty zircon grains were analyzed in this study. Most results deviated from the concordia line, but all data could fit a line, showing a lower intercept age of 428 ± 6.6 Ma (MSWD = 0.77) (Figure 4b), which represents the best estimate for the eruption time of the basalt.

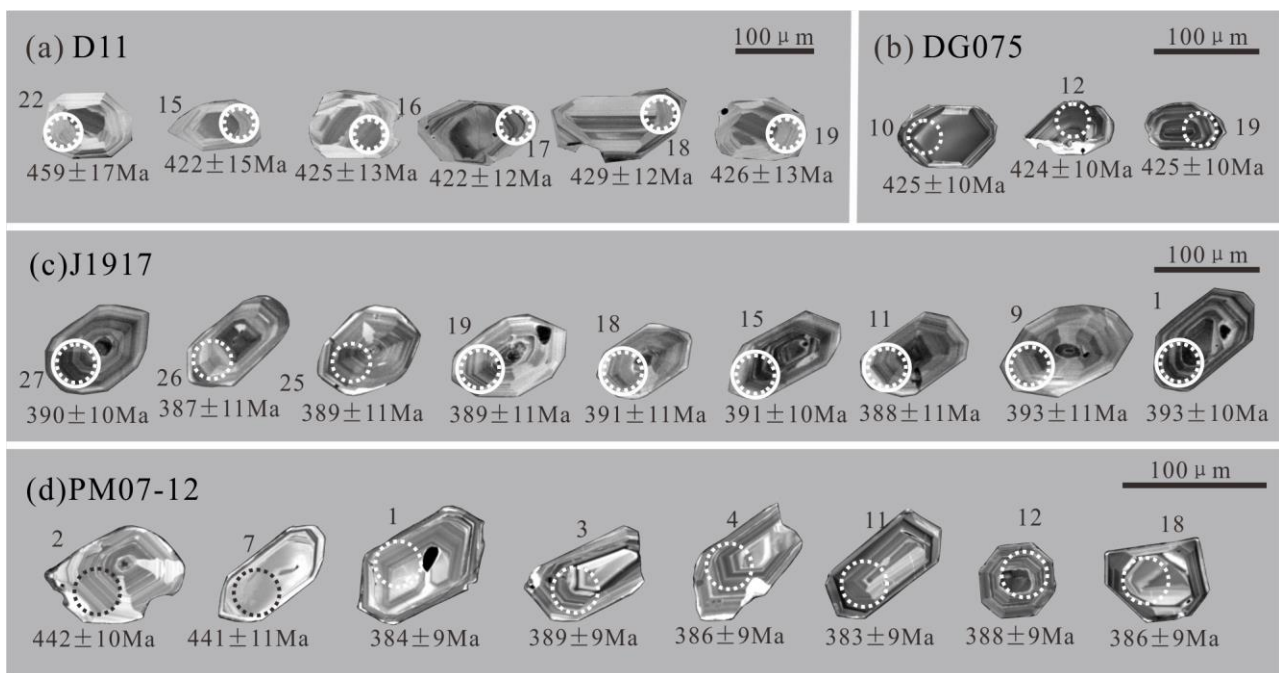


Figure 3. Representative CL images of zircons from the Middle Silurian–Middle Devonian magmatic rocks in the Yitong area. (a) CL image of zircons from sample D11. (b) CL image of zircons from sample DG075. (c) CL image of zircons from sample J1917. (d) CL image of zircons from sample PM07-12. The solid line circle is the Hf isotope analysis point; the dotted line circle is the U-Pb age analysis point. The numbers show the ages of the zircons (Ma) and the $\epsilon_{\text{Hf}}(t)$ values.

Sample J1917 is an andesite from the Fangniugou volcanic rocks. These zircons are tabular and short columnar, with grain sizes of 50–100 μm and length/width ratios of 1:1 to 2:1. The CL images (Figure 3c) show that these zircon grains have typical zonal textures and Th/U ratios of 0.56–1.47, suggesting magmatic zircons. Twenty-nine zircon grains in this sample were dated, with all results lying on or near the concordia line. The analyses give a weighted mean $^{206}\text{Pb}/^{238}\text{U}$ age of 388.4 ± 3.9 Ma (MSWD = 0.23) (Figure 4c), representing the best estimate for the eruption time of the andesite.

Sample PM07-12 is a metamorphic olivine-bearing basalt, from the Fangniugou volcanic rocks. These zircons are tabular and short columnar (Figure 3d), with grain sizes of 50–120 μm and length/width ratios of 1:1 to 3:1. The CL images show that these zircon grains have typical zonal textures and Th/U ratios of 0.45–1.35, suggesting magmatic zircons. Eighteen zircon grains in this sample were dated, with all results lying on or near the concordia line. Of these, 13 zircon grains have $^{206}\text{Pb}/^{238}\text{U}$ ages of 372–389 Ma, with a weighted mean $^{206}\text{Pb}/^{238}\text{U}$ age of 384.1 ± 4.9 Ma (MSWD = 0.33) (Figure 4d), representing the eruption time of the basalt. Another 4 zircon grains have $^{206}\text{Pb}/^{238}\text{U}$ ages of 446 ± 10 Ma, 442 ± 10 Ma, 441 ± 11 Ma, and 418 ± 11 Ma, most likely representing xenocrystic zircon ages.

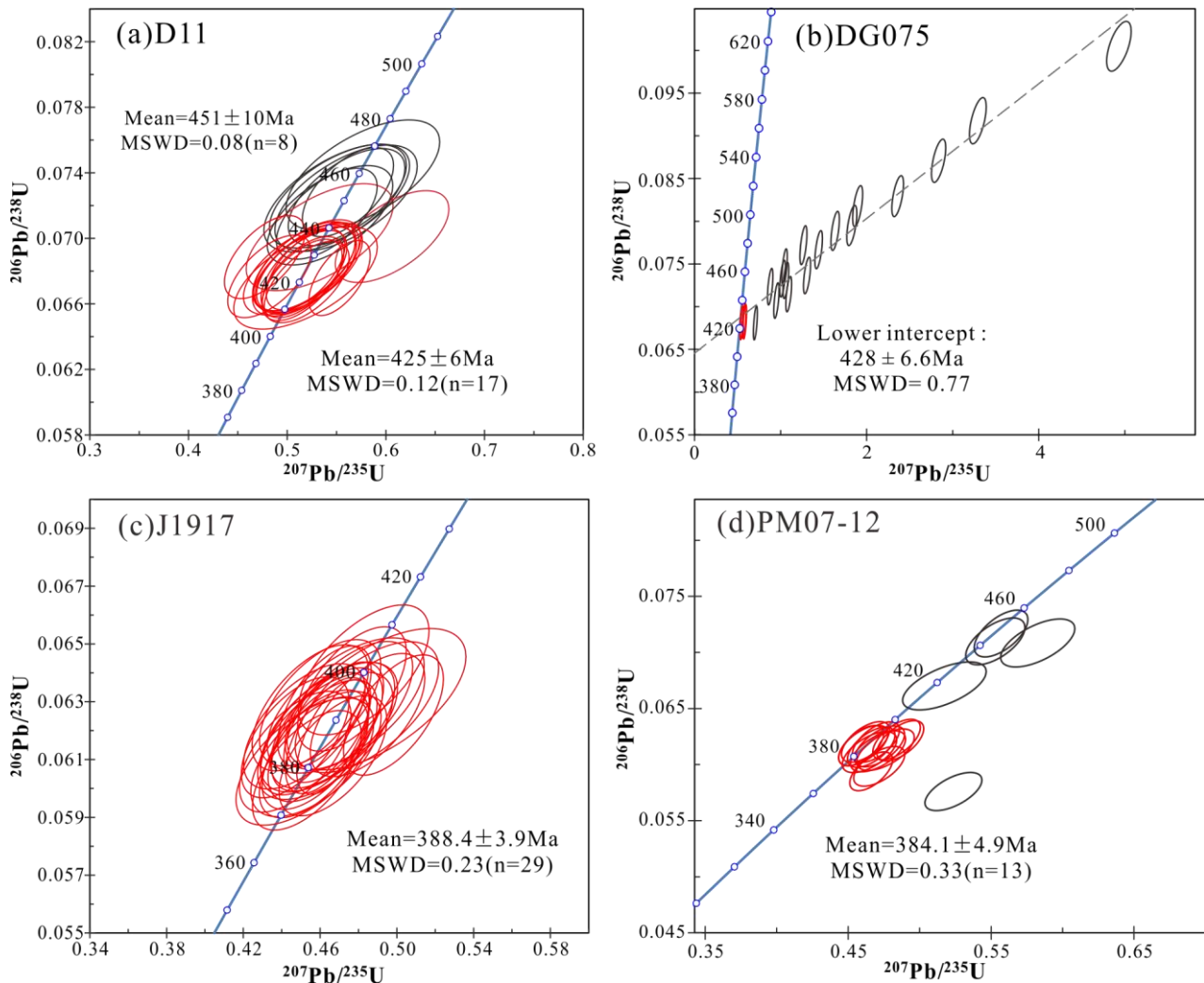


Figure 4. Zircon U-Pb concordia diagrams from the Middle Silurian–Middle Devonian magmatic rocks in the Yitong area. (a) Zircon U-Pb concordia diagrams from sample D11. (b) Zircon U-Pb concordia diagrams from sample DG075. (c) Zircon U-Pb concordia diagrams from sample J1917. (d) Zircon U-Pb concordia diagrams from sample PM07-12. Data-point error ellipses are 1 sigma. Age errors are 95% confidence.

4.2. Whole-Rock Major and Trace Elements Analysis

The whole-rock major and trace elements analysis results are shown in Supplementary Table S2.

The K_2O/Na_2O ratios of Late Silurian tonalite (D11) samples are 0.44–0.59, indicating that they are relatively enriched in Na and depleted in K. Their A/CNK ratios range from 0.91 to 1.00, showing metaluminous signatures. In the An-Ab-Or classification diagram (Figure 5a), data for the samples are located within the field of tonalite. As revealed by the rock series discrimination diagram (Figure 5d), the samples all fall into the calc-alkaline zone. The samples have relatively higher ΣREE contents (167.38–180.81 ppm), exhibiting LREE enrichment ($La_N/Yb_N = 2.40\text{--}3.32$) with slightly negative Eu anomalies ($Eu/Eu^* = 0.77\text{--}0.84$) (Figure 6a). According to the parameters proposed by Irber [76] and Monecke [77], Ce_N/Ce^* and Pr_N/Pr^* of the tonalites are slightly less than 1, T1 is slightly greater than 0, and t1 is slightly less than 1 (Table S2), indicating that the first group of rare earth elements (La, Ce, Pr, and Nd) show a weak W-type tetrad effect. Tb_N/Tb^* , Dy_N/Dy^* , Tm_N/Tm^* , and Yb_N/Yb^* are significantly greater than 1, T3 is greater than 0, t3 and t4 are greater than 1 (Table S2), all indicating that the third group (Ga, Tb, Dy, and Ho) and the fourth group (Er, Tm, Yb, and Lu) of rare earth elements show a significant M-type tetrad

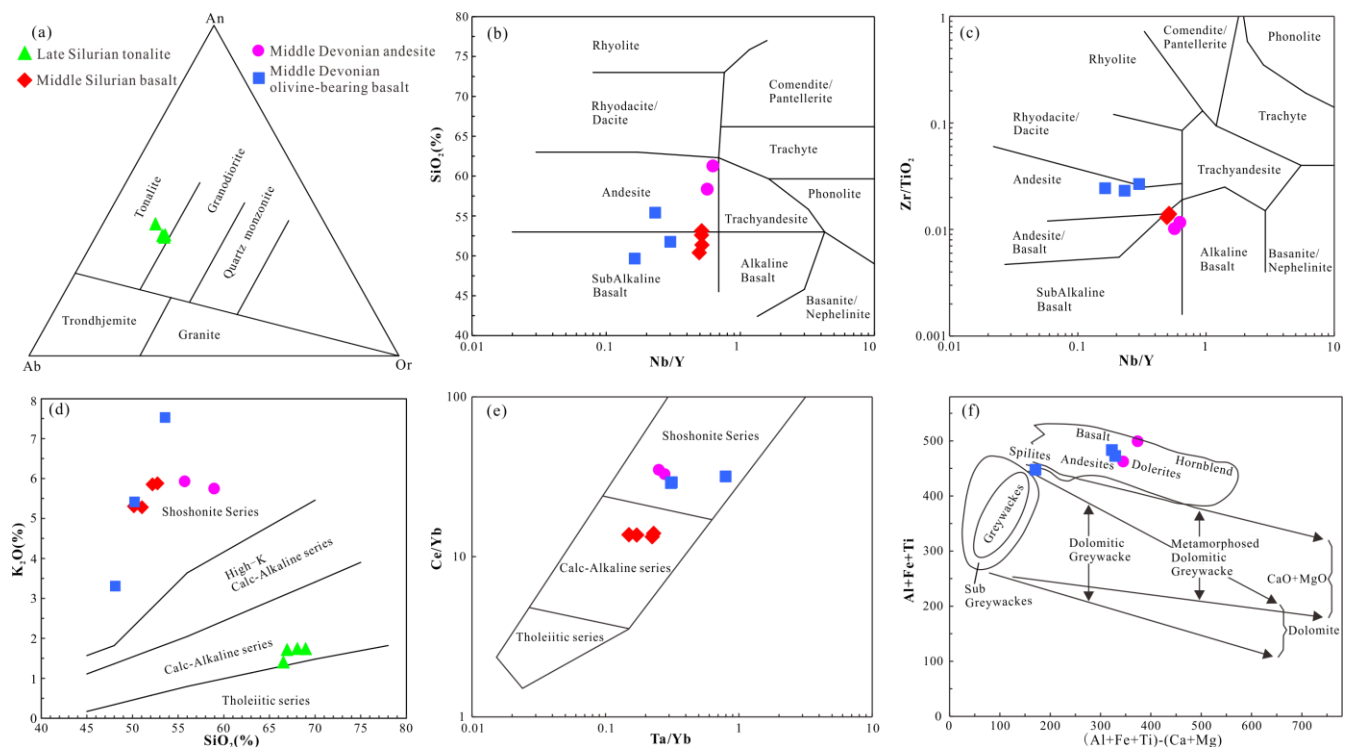


Figure 5. (a) An-Ab-Or [78], (b) SiO₂ versus Nb/Y [79], (c) Zr/TiO₂ versus Nb/Y [79], (d) K₂O versus SiO₂ [80], (e) Ce/Yb versus Ta/Yb [81], and (f) Al + Fe + Ti versus (Al + Fe + Ti) + (Ca + Mg) [82] diagrams for the Middle Silurian–Middle Devonian magmatic rocks in the Yitong area.

The K₂O/Na₂O ratios of Middle Silurian basalt (DG075) samples are 1.24–1.57, indicating that they are relatively enriched in K and depleted in Na. Their A/CNK ratios range from 0.58 to 0.64, showing metaluminous signatures. Their Rittmann index σ (9.70–11.75) suggests peralkaline characteristics. The basalt samples dominantly plot in the shoshonite series field (Figure 5d). In the SiO₂ vs. Nb/Y and Zr/TiO₂ vs. Nb/Y diagrams (Figure 5b,c), the data for the samples are located within the field of sub-alkaline basalt. They fall within the calc-alkaline series on the Ce/Yb vs. Ta/Yb diagram (Figure 5e) due to their low Ce content. The samples have relatively higher REE contents (145.15–152.30 ppm), exhibiting LREE enrichment ($La_N/Yb_N = 5.89–6.16$) with positive Eu anomalies ($Eu/Eu^* = 1.10–1.29$) and negative Ce anomalies ($Ce/Ce^* = 0.68–0.74$) (Figure 6a). The trace element spider plot illustrates that the samples are relatively enriched in Rb, Ba, Th, U, and K (LILEs), and depleted in Nb, Ta, Sr, P, and Ti (HFSEs) (Figure 6b).

The K₂O/Na₂O ratios of Middle Devonian andesite (J1917) samples are 57.74–150.66, indicating that they are enriched in K and depleted in Na. Their A/CNK ratios range from 2.03 to 2.10, showing peraluminous signatures. The andesite samples plot in the shoshonite series field (Figure 5d,e) and in the andesite and sub-alkaline basalt regions on the SiO₂ vs. Nb/Y and Zr/TiO₂ vs. Nb/Y diagrams (Figure 5b,c). The samples have relatively higher REE contents (171.29–188.49 ppm), exhibiting LREE enrichment ($La_N/Yb_N = 12.15–14.54$) with no Eu anomalies ($Eu/Eu^* = 0.91–0.95$) and negative Ce anomalies ($Ce/Ce^* = 0.78–0.87$) (Figure 6c). The trace element spider plot illustrates that the samples are relatively enriched in Rb, Th, U, and K (LILEs) and depleted in Nb, Ta, Sr, Zr, and HREEs (Figure 6d).

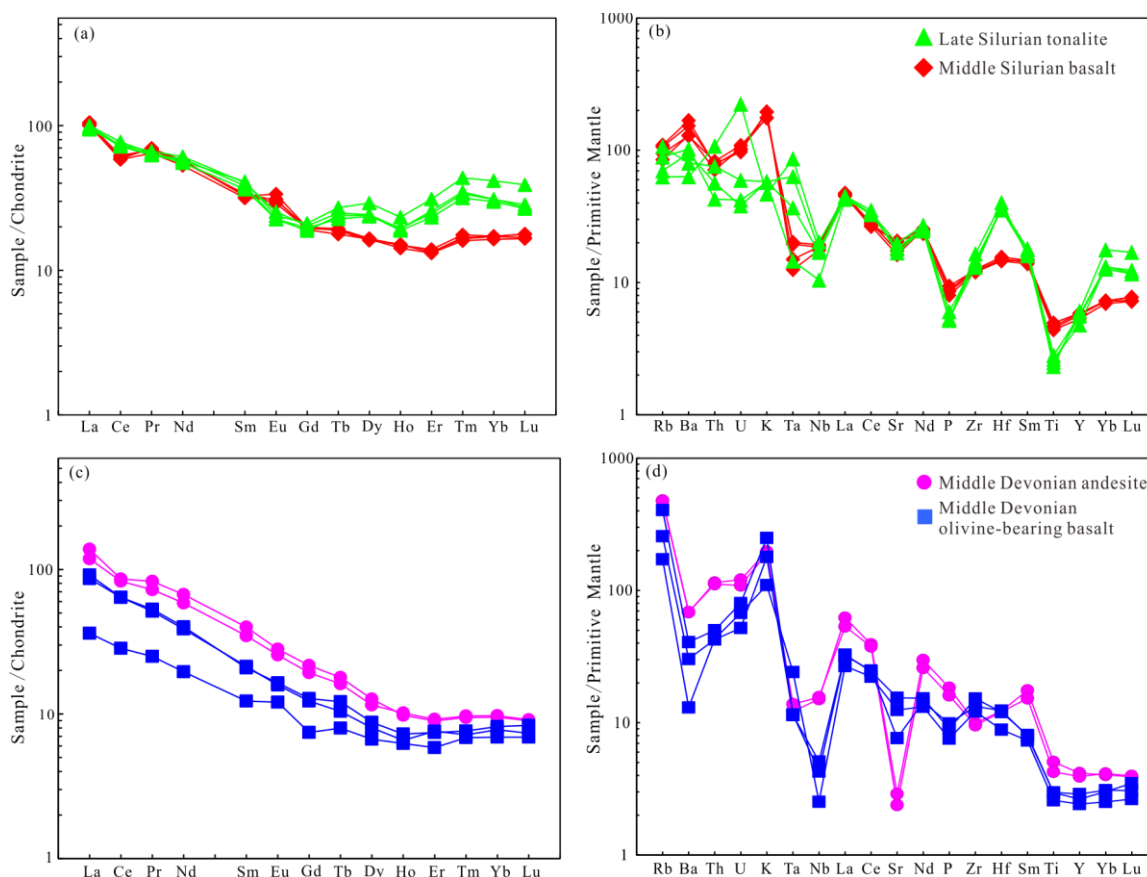


Figure 6. Chondrite-normalized REE patterns (a,c) (normalizing values after Boynton [83]), and primitive-mantle-normalized trace element spider diagrams (b,d) (normalizing values after Sun and Mc Donough [84]) for the Middle Silurian–Middle Devonian magmatic rocks in the Yitong area.

The K_2O/Na_2O ratios of the Middle Devonian metamorphic olivine-bearing basalt (PM07-12) samples are 13.25–24.14, indicating that they are enriched in K and depleted in Na. According to the $(Al + Fe + Ti)$ vs. $(Ca + Mg)$ diagram (Figure 5f), the samples predominantly classify within the regions of basalt and basaltic andesite volcanic rocks, suggesting that the protolith was an intermediate to mafic volcanic rock. Their A/CNK ratios range from 0.84 to 1.07, showing metaluminous–weakly peraluminous signatures. The andesite samples plot in the shoshonite series field (Figure 5d) and in the sub-alkaline basalt and andesite regions on the SiO_2 vs. Nb/Y and Zr/TiO_2 vs. Nb/Y diagrams (Figure 5b,c). The samples have relatively lower REE contents (93.52–106.89 ppm), exhibiting LREE enrichment ($La_N/Yb_N = 9.77$ – 10.23) with positive Eu anomalies ($Eu/Eu^* = 1.12$ – 2.12) and no Ce anomalies ($Ce/Ce^* = 0.92$ – 1.02) (Figure 6c). The trace element spider plot illustrates that the samples are relatively enriched in Rb and K and depleted in Ba, Th, U, Nb, Ta, Sr, P, Ti, and HREEs (Figure 6d).

4.3. Zircon Lu-Hf Isotopes

Based on LA-ICP-MS zircon U-Pb dating of Late Silurian tonalite and Middle Devonian andesite in the Yitong area, this study conducted in situ zircon Hf isotope analysis of some zircons from the dated samples (Figure 7a). The analytical results are shown in Supplementary Table S3.

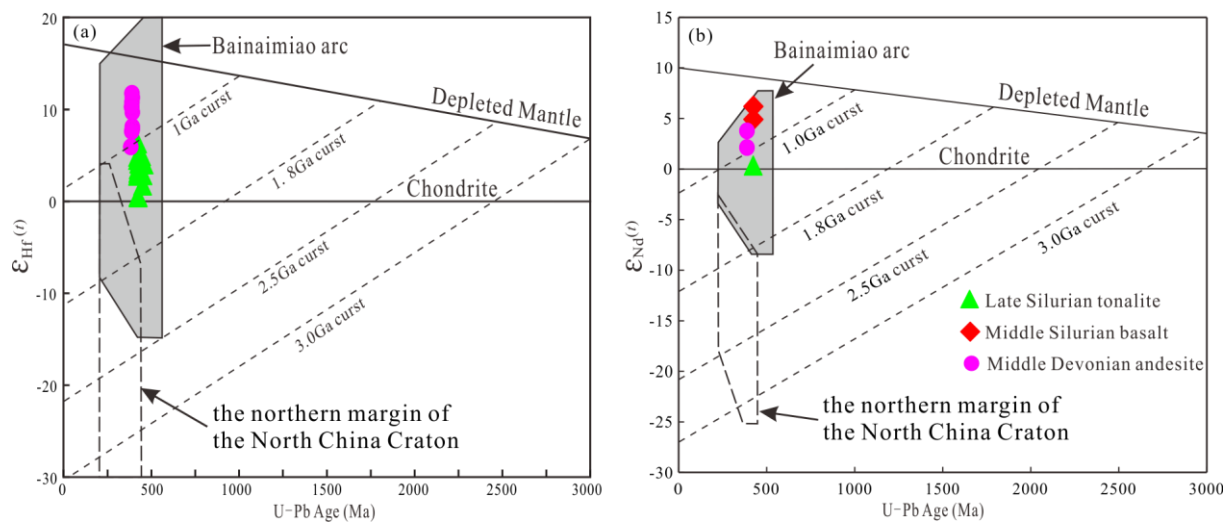


Figure 7. (a) $\epsilon_{\text{Hf}}(t)$ versus U-Pb age for zircons [85], and (b) $\epsilon_{\text{Nd}}(t)$ versus U-Pb age for zircons [86] of the Middle Silurian–Middle Devonian magmatic rocks in the Yitong area.

Sixteen zircons from Late Silurian tonalite sample D11 that represented the younger group gave $\epsilon_{\text{Hf}}(t)$ values of +0.44–+6.31. They show single-stage Hf model ages (T_{DM1}) and two-stage Hf model ages (T_{DM2}) of 790–1027 Ma and 1005–1379 Ma, respectively. Ten zircons from Middle Devonian andesite sample J1917 gave $\epsilon_{\text{Hf}}(t)$ values of +5.90–+11.73. They show single-stage Hf model ages (T_{DM1}) and two-stage Hf model ages (T_{DM2}) of 552–796 Ma and 636–1001 Ma, respectively.

4.4. Whole-Rock Sr-Nd Isotopes

Measured and age-corrected initial isotopic ratios of Sr and Nd are presented in Supplementary Table S4. The Sm, Nd, Rb, and Sr contents of these rocks are given in Supplementary Table S2.

The Late Silurian tonalite sample has initial $^{87}\text{Sr}/^{86}\text{Sr}$ ratios (I_{Sr}) of 0.70646 and $\epsilon_{\text{Nd}}(t)$ values of +0.35. In contrast, the Middle Silurian basalt samples possess lower initial $^{87}\text{Sr}/^{86}\text{Sr}$ ratios ($I_{\text{Sr}} = 0.70499\text{--}0.70508$) and distinctly higher positive $\epsilon_{\text{Nd}}(t)$ values (+4.91 to +6.18) (Figure 7b and Figure 9d). The Middle Devonian andesites have positive $\epsilon_{\text{Nd}}(t)$ values of +2.11 to +3.77, but initial $^{87}\text{Sr}/^{86}\text{Sr}$ ratios ($I_{\text{Sr}} = 0.66800\text{--}0.67546$) are too low to have any genetic significance. All samples exhibit positive $\epsilon_{\text{Nd}}(t)$ values, which is consistent with the Bainaimiao arc magmatic rocks in the CAO (Figure 7b). The Middle Silurian basalts and Middle Devonian andesites have Neoproterozoic Nd model ages ($T_{\text{DM1}} = 647\text{--}956$ Ma; $T_{\text{DM2}} = 663\text{--}964$ Ma), whereas the Late Silurian tonalite has Mesoproterozoic Nd model age ($T_{\text{DM1}} = 1119$ Ma; $T_{\text{DM2}} = 1138$ Ma).

5. Discussions

5.1. Silurian to Devonian Magmatism in the Eastern Section of the Northern Margin of the NCC

Previous studies [29,32,43,44,48,68], indicate that the 424 ± 6 Ma Ximangzhang pluton underwent multiple episodes of magmatism during the Late Ordovician to Early Silurian (448–438 Ma), Late Silurian (425–419 Ma), and Early Devonian (414 Ma), forming a magmatic complex. The Fangniugou volcanic rocks emerged in the Middle Silurian to the Late Devonian, which was marked by multiple volcanic episodes at 428–425 Ma, 419 Ma, 404–400 Ma, 390–384 Ma, and 375 Ma.

In recent years, Cambrian–Devonian geological bodies have been reported successively from the eastern section of the northern margin of the NCC in Faku-Kaiyuan, Liaoning Province, and Gongzhuling-Liaoyuan-Zhangjiatun-Yanbian, Jilin Province (Figure 8) [29,43,44,48,56,64,68–70]. The Early Paleozoic magmatism in this region extended from the Late Cambrian to the Late Silurian, with peaks observed at 494 Ma, 486 Ma, 475 Ma, 467 Ma,

459 Ma, 438 Ma, and 422 Ma. These peaks resemble those of the Early Paleozoic Bainaimiao arc belt magmatic rocks [32], suggesting that the subduction-accretionary complex belt in the Faku-Yanji area is an extension of the Bainaimiao arc belt in the east. Combined with previous data, the Silurian magmatism in the northern margin of the NCC ranges from 443 to 419 Ma, and the Devonian magmatism ranges from 414 to 375 Ma (Table 2). The Silurian (443–419Ma) magmatism is frequent and distributed along the north margin of the NCC in an east–west direction, mainly exposed in the Faku, Gongzhuling, Yitong, Zhangjiatun, and Yanbian areas. The lithology is mainly intermediate-acid magmatic rocks, including andesite, quartz diorite, tonalite, granodiorite, rhyodacite, granite, rhyolite, etc. [29,32,43,44,48,56,57,87,88]. Mafic rocks are rarely exposed, only found in the Yitong area, as shoshonitic basalt. The Devonian (414–375 Ma) magmatism is weaker, exposed in Faku, Changtu, Gongzhuling, and Liaoyuan, with lithology mainly including granodiorite, rhyolite, rhyolitic tuff, dacite, monzogranite, etc., as well as a small amount of basalt and basaltic andesite [29,43,68–71,89].

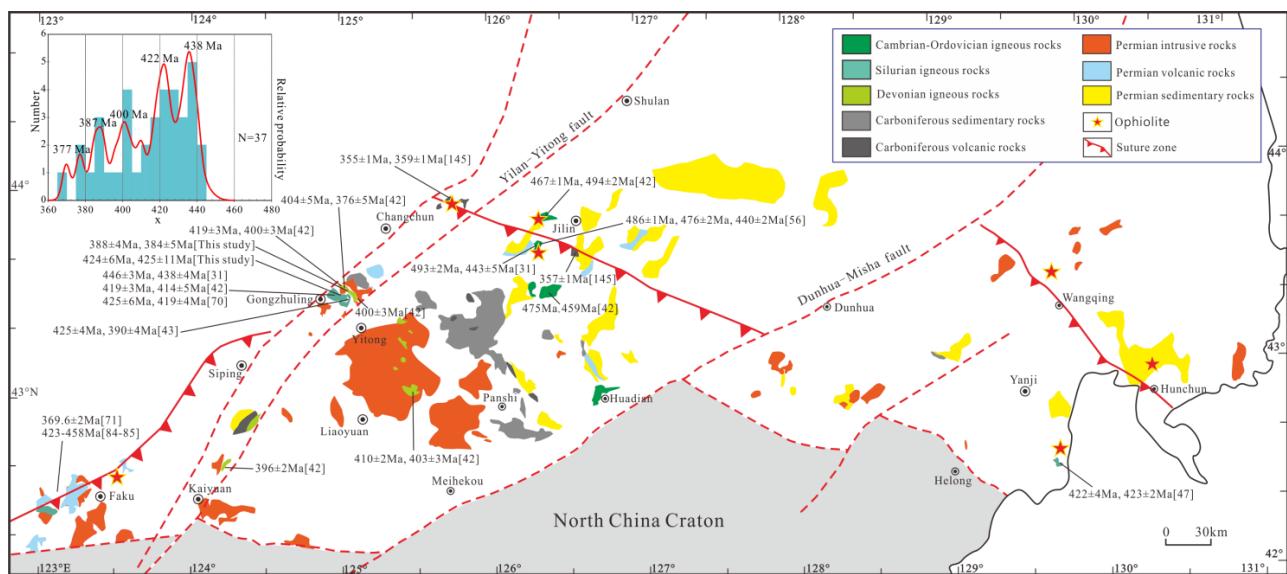


Figure 8. Distribution of Paleozoic magmatic rocks and strata from the Faku–Yanji area in the eastern segment of the northern margin of the NCC [17,29,31,42,43,47,56,70,71,84,85,89–91].

Table 2. Geochronological data for the Silurian–Devonian magmatic rocks in the eastern segment of the northern margin of the NCC.

Rocks	Sampling Location	Method	Ages (Ma)	References
Tonalite	E126°17'41", N43°41'21"	LA-ICP-MS	443 ± 5	[56]
Tonalite	Zhangjiatun	LA-ICP-MS	440 ± 2	[57]
Quartz diorite	E124°56'15", N43°27'38"	LA-ICP-MS	438 ± 4	[32]
Granodiorite	E123°14'51", N42°32'59"	LA-ICP-MS	438 ± 4	[32]
Tonalite	E123°14'27", N42°32'41"	SHRIMP	437 ± 3	[87]
Granite	E123°13'59", N42°33'56"	LA-ICP-MS	436 ± 2	[32]
Granodiorite	E123°14'17", N42°32'25"	LA-ICP-MS	436 ± 3	[32]
Granodiorite	E123°13'18", N42°33'28"	LA-ICP-MS	434 ± 3	[32]
Granodiorite	E123°13'55", N42°32'20"	SHRIMP	433 ± 3	[88]
Granodiorite (adakite)	E123°02'47", N42°31'20"	SHRIMP	432 ± 3	[87]
Andesite	E125°01'51", N43°28'00"	LA-ICP-MS	426 ± 4.8	[29]
Dacite	E125°08'51", N43°28'04"	LA-ICP-MS	425 ± 4	[44]
Tonalitic mylonite	E124°58'29", N43°29'40"	LA-ICP-MS	425 ± 6	[29]
Basalt	E125°01'31", N43°29'37"	LA-ICP-MS	428 ± 6.6	This study
Tonalite	E124°56'07", N43°27'42"	LA-ICP-MS	424 ± 6	This study

Table 2. Cont.

Rocks	Sampling Location	Method	Ages (Ma)	References
Felsic mylonite	E123°10'50", N42°35'05"	SHRIMP	423 ± 5	[88]
Tonalite	E129°41'11", N42°33'28"	LA-ICP-MS	423 ± 2	[48]
Tonalite	E129°40'37", N42°33'12"	LA-ICP-MS	422 ± 4	[48]
Rhyolite	E125°02'37", N43°29'38"	LA-ICP-MS	419 ± 3	[43]
Granodiorite	E124°56'03", N43°27'44"	LA-ICP-MS	419 ± 3	[43]
Tonalite	E124°56'15", N43°28'04"	LA-ICP-MS	419.5 ± 4	[29]
Granodiorite	E124°58'32", N43°29'40"	LA-ICP-MS	414 ± 5	[43]
Rhyolitic tuff	E125°26'44", N43°01'59"	LA-ICP-MS	410 ± 2	[43]
Rhyolitic tuff	E125°27'50", N43°02'15"	LA-ICP-MS	403 ± 3	[43]
Basalt	Faku	LA-ICP-MS	405 ± 5	Shi et al. (unpublish)
Rhyolitic tuff				
rhyolitic crystal tuff	E125°00'51", N43°31'52"	LA-ICP-MS	404 ± 4.5	[29]
rhyolitic crystal tuff				
Dacite	E125°01'40", N43°53'11"	SHRIMP	402 ± 4	[68]
Monzogranite	E124°57'29", N43°31'04"	LA-ICP-MS	400 ± 2	[43]
Monzogranite	E124°54'22", N42°07'15"	LA-ICP-MS	396 ± 2	[43]
Rhyolite	E124°59'39", N43°28'27"	LA-ICP-MS	390 ± 4	[44]
Biotite monzogranite	E124°16'44", N42°48'08"	LA-ICP-MS	389 ± 2	[70]
Rhyolite crystal tuff	E124°27'13", N42°54'15"	LA-ICP-MS	385 ± 2	[70]
Andesite	E125°03'24", N43°30'29"	LA-ICP-MS	388 ± 4	This study
Metamorphic olivine-bearing basalt	E125°04'12", N43°30'28"	LA-ICP-MS	384 ± 5	This study
Monzogranite	E124°15'47", N42°49'01"	LA-ICP-MS	377 ± 2	[70]
Rhyolite	E125°01'20", N43°32'00"	LA-ICP-MS	375.5 ± 5	[29]
High-Mg andesite	E123°33'19", N43°39'13"	LA-ICP-MS	369.6 ± 2	[89]

5.2. Petrogenesis and Source Characteristics

5.2.1. Middle–Late Silurian Magmatic Rocks

The Middle–Late Silurian magmatic rocks display relatively weak metamorphism and deformation, with a low loss on ignition (LOI = 0.50–0.75), indicating minimal alteration effects. These geochemical characteristics make them well-suited for investigating their petrogenesis and source features.

The Late Silurian tonalites have high contents of SiO₂ and Na₂O, and low contents of K₂O, MgO, FeOT, and TiO₂, with an A/CNK ratio of 0.91–1.00, indicative of I-type granites. In the Na₂O vs. K₂O diagram (Figure 9a), the tonalite samples fall within the zone of the I-type granite. Additionally, in the petrogenetic discrimination diagrams (Figure 9b), all tonalite samples fall within the zone of unfractionated granitoids. These characteristics are consistent with those of metaluminous calc-alkaline I-type granitoids. They exhibit enrichment in Rb, Ba, Th, U, and K (LILEs) and depletion in Nb, Sr, P, and Ti (HFSEs), displaying magmatic arc features [19,92,93]. The explanations for the tetrad effect of rocks include mineral crystallization [94,95], late-stage magma-fluid interactions [76,96,97], or inheritance from the parental magma [76,97]. According to published papers [29,43], the Ximangzhang tonalites do not exhibit tetrad effects, indicating that this characteristic is not a feature of its primary magma. The low Zr/Hf (12.81–14.99) and Y/Ho (15.41–18.83) ratios in tonalites cannot be explained by mineral crystallization [98,99]. Crust-derived magmas that have undergone significant magma-hydrothermal exchange typically exhibit lower Zr/Hf ratios (<20) [76]. The Nb/Ta ratio (4.11–12.49, average 7.38) in tonalite is similar to the differentiated continental crust (11) [100]. Therefore, the REE anomalies may be caused by magma-fluid interactions. Increasing La concentrations correspond with a rise in the La/Sm ratio, indicative of partial melting processes during their formation. The absence of pronounced Sr and Eu anomalies further supports the partial melting of plagioclase in the source material. The tonalites have low Cr (24.70–30.82 ppm) and Ni (5.34–6.56 ppm) content and Mg# (39.26–43.79) values, indicating a crustal source. Their

La/Sm ratios between 3.72 and 4.34 (average 3.98) suggest a moderate degree of crustal contamination, given that ratios above 4.5 typically indicate strong contamination, while those below 2 suggest primary compositions [101]. Additionally, the tonalites display high Ba/Th (48.35–196.86, average 117.57) and Ba/La (14.27–24.49, average 19.79) ratios, but low Th content (3.63–9.13 ppm) and Th/Yb ratios (0.56–1.05), implying that slab-derived fluids primarily influenced the source of these Late Silurian magmatic rocks [102], with lesser contributions from sediments or melts. The Rb/Ba vs. Rb/Sr diagram (Figure 9c) shows that the source material for the tonalite is predominantly basalt. The $\epsilon_{\text{Nd}}(t)$ vs. I_{Sr} diagram (Figure 9d) indicates that the magmas are composed of approximately 70–75% basalt and 25–30% lower continental crust. The $\epsilon_{\text{Nd}}(t)$ value of tonalite is +0.35, with a two-stage model age of 1138 Ma, and zircon $\epsilon_{\text{Hf}}(t)$ values ranging from +0.44 to +6.31, with a two-stage model age ranging from 1005.0 to 1379.5 Ma. These characteristics indicate that the tonalite predominantly originated from partial melting of Mesoproterozoic accreted lower crustal material (basalt), and magma ascent was accompanied by contamination with lower crustal material.

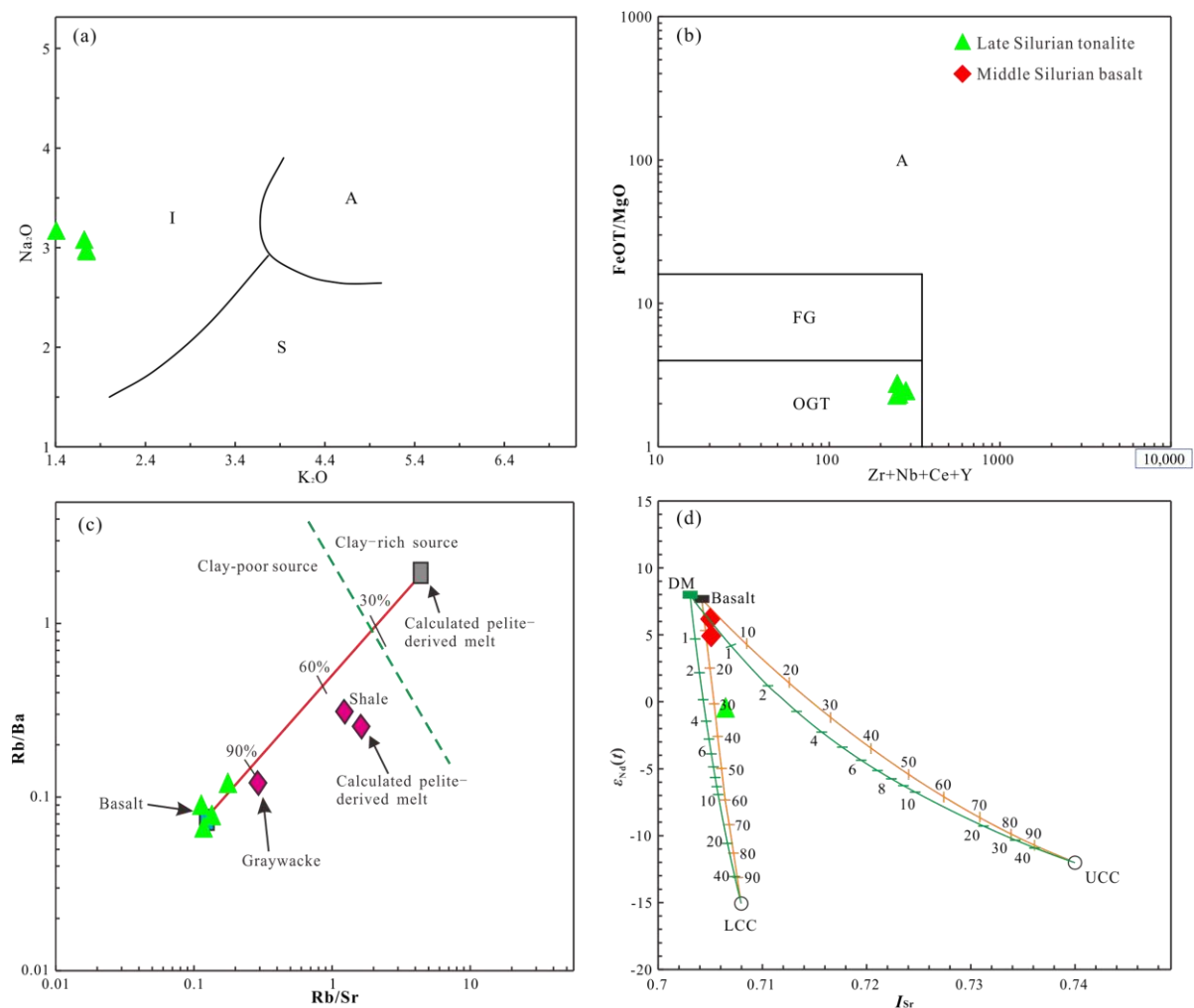


Figure 9. (a) Na₂O versus K₂O diagram [103], (b) FeOT/MgO versus (Zr + Nb + Ce + Y) diagram [104], (c) Rb/Ba versus Rb/Sr diagram (The red solid line represents the mixing curve between basalt- and pelite-derived melts; The green dashed line divides strongly peraluminous granites derived mostly from clay-poor sources from those formed mostly from clay-rich source rocks.) [105], and (d) $\epsilon_{\text{Nd}}(t)$ versus I_{Sr} diagram [105] for the Middle Silurian–Middle Devonian magmatic rocks in the Yitong area. FG: fractionated granitoid; OGT: unfractionated granitoid; I: I-type granitoid; S: S-type granitoid; A: A-type granitoid; DM: depleted mantle; LCC: lower continental crust; UCC: upper continental crust.

The Middle Silurian basalts have low contents of SiO_2 , P_2O_5 , TiO_2 , and Na_2O and high contents of Al_2O_3 , FeO , CaO , and K_2O , with a $\text{K}_2\text{O}/\text{Na}_2\text{O}$ ratio of 1.24–1.57. Notably, these basalts contain primarily K-feldspar phenocrysts, with σ values ranging from 9.70 to 11.75, and CIPW norm calculations indicating the presence of nepheline ($\text{Ne} = 7.41\text{--}10.69$), but alkaline minerals are absent in thin section observations. Positioned within the subalkaline basalt region in the SiO_2 vs. Nb/Y and Zr/TiO_2 vs. Nb/Y diagrams (Figure 5b,c), these samples are identified as shoshonitic rocks rather than typical alkaline rocks. The ratios of incompatible elements, largely unchanged by fractional crystallization, remain constant during the partial melting of the mantle, thereby serving as indicators of magma source characteristics [106]. Geochemical analysis reveals an average Lu/Yb ratio of 0.15–0.16, closely aligned with the typical mantle-derived magmatic value of 0.14–0.15 [107], and an average Nb/Ta ratio of 19.80, approaching the mantle standard of 17.5 [84,106], affirming their mantle-derived magmatic nature. Positive $\epsilon_{\text{Nd}}(t)$ values ranging from +4.91 to +6.18 further affirm a mantle origin. Additionally, high ratios of La/Ta (37.94–60.22 > 22) and La/Nb (2.27–2.47 > 1.7), alongside low Zr/Ba (0.12–0.16) and La/Ba (0.03–0.04) ratios, point to a genesis within the lithospheric mantle, modified by subduction processes [108–112]. These basalts also exhibit high Ba/Th (128.08–177.84) and Ba/La (27.88–36.84) ratios and lower La/Sm (4.78–5.03) and Th/Yb (1.69–1.97) ratios, indicative of a mantle-derived magmatic source predominantly influenced by slab dehydration [102]. They are enriched in Rb, Ba, Th, U, K, and LREE, yet depleted in Nb, Ta, Sr, P, and Ti, characteristic of island arc magmatic rocks [19], suggesting an origin from the lithospheric mantle that has been metasomatized by subduction fluids [113]. Furthermore, relatively low Cr (67.60–70.51 ppm), Ni (38.95–40.13 ppm), and Co (17.96–19.97 ppm) contents and Mg# (32.15–34.95) values suggest a significant evolutionary process during its formation [114], such as fractional crystallization of olivine or pyroxene, or crustal contamination. Their average Rb/Sr ratio of 0.16 distinctly reflects a mixed mantle-crust source, consistent with the typical mantle-crust mixed source magmatic Rb/Sr ratio range of 0.05–0.50 [106]. Island arc volcanic rocks often exhibit a characteristic negative anomaly in Ce concentrations [115]. The samples have negative Ce anomaly (0.68–0.74) and low Ce/Th ratios (6.97–7.89), further suggesting the incorporation of subducted sediment melts into the source. The $\epsilon_{\text{Nd}}(t)$ vs. I_{sr} diagram (Figure 9d) indicates that the magma mainly originated from a depleted mantle with some crustal material addition. The Nd isotope single-stage model age (T_{DM1}) ranges from 647 to 758 Ma, which represents the mixed age of juvenile crust and older crust, suggesting the presence of a Proterozoic crystalline basement in the study area. Collectively, these features indicate that the Middle Silurian basalts primarily originated from depleted mantle magmas metasomatized by subduction fluids, supplemented by a small amount of subducted sediments and crustal materials.

5.2.2. Middle Devonian Volcanic Rocks

The Middle Devonian volcanic rocks have undergone weak metamorphism and deformation with a slightly higher loss on ignition ($\text{LOI} = 2.94\text{--}4.78$). Therefore, to discern the rock origins and source characteristics, less mobile lithogenic elements along with rare earth elements and high field strength elements, which are less affected by metamorphism and alteration, are primarily utilized [116].

The Middle Devonian volcanic rocks have low SiO_2 , TiO_2 , and Na_2O content and high K_2O content, and a high $\text{K}_2\text{O}/\text{Na}_2\text{O}$ ratio with a wide range of variation in Al_2O_3 content (ranging from 13.65 to 17.50 wt%). In the SiO_2 vs. Nb/Y and Zr/TiO_2 vs. Nb/Y diagrams (Figure 5b,c), these volcanic rocks primarily fall into the subalkaline basalt and andesite zones, indicating that the K-rich and Na-poor characteristics of the samples are a result of alteration. The samples are enriched in LILEs such as Rb, K, and LREEs and are depleted in Nb, Ta, Sr, and HREEs, showing geochemical characteristics similar to those of arc volcanics [117–121].

The Zr/Hf ratio of these volcanic rocks (28.74–49.78, average 38.59) is close to that of mantle-derived magmas (39) [122]; their average Lu/Yb ratio (0.14–0.17) is also close to

the average mantle-derived magma value (0.14–0.15) [107], affirming their mantle-derived magmatic nature. The volcanic rocks have positive $\epsilon_{\text{Nd}}(t)$ values (+2.11 to +3.77), also indicating mantle-derived magma. Additionally, high ratios of La/Ta (18.57–85.64, average 52.79 > 22) and La/Nb (3.29–10.22 > 1.7), alongside low Zr/Ba (0.22–1.50) and La/Ba (0.08–0.20) ratios, point to a genesis within the lithospheric mantle, modified by subduction processes [108–112].

It is generally believed that the fluids or melts formed during the subduction of oceanic crust and sediments metasomatize the overlying mantle wedge, resulting in partial melting and the formation of island arc magma [123,124]. The addition of subduction zone fluids significantly lowers the Ce/Pb and Nb/U ratios of magmas originating from depleted mantle [125]. The Middle Devonian volcanic rocks have Nb/U (1.27–4.86) and Ce/Pb (0.66–10.30) ratios lower than those of typical depleted mantle (Nb/U = 47 ± 10 , Ce/Pb = 25 ± 5) [126], suggesting the addition of subduction zone fluids to the magma source. Sample J1917 has low Ce/Th ratios (7.07–7.13) and a Ce negative anomaly (0.78–0.87), suggesting the addition of subducted sediment melts to the source. Sample PM07 has higher Ce/Th ratios (10.36–11.98) and no Ce anomaly (0.92–1.02), suggesting no addition of reduced sediment melts in the source. The volcanic rocks have low Cr (2.35–10.09 ppm) and Ni (2.74–3.96 ppm) content and Mg# values (21.24–47.39), suggesting they may have undergone fractional crystallization of olivine and pyroxene, or crustal contamination [114]. Typically, the addition of crustal material leads to an increased abundance of LILEs (Rb, Ba, Th, etc.) and decreased content of HFSEs (Nb, Ta, Ti, etc.). Important indicators of crustal contamination include $(\text{Th}/\text{Nb})_{\text{PM}} \gg 1$ [127], $\text{La}/\text{Nb} > 1$ [128], and La/Sm values (>4.5) [101]. The Middle Devonian volcanic rocks exhibit $(\text{Th}/\text{Nb})_{\text{PM}} = 7.12$ –17.02, $\text{La}/\text{Nb} = 3.29$ –10.22, and $\text{La}/\text{Sm} = 5.42$ –6.29, suggesting a limited degree of crustal contamination.

In the $\epsilon_{\text{Hf}}(t)$ vs. t and $\epsilon_{\text{Nd}}(t)$ vs. t diagrams (Figure 7a,b), the Middle Devonian volcanic rock samples fall within the $\epsilon_{\text{Hf}}(t)$ and $\epsilon_{\text{Nd}}(t)$ ranges of the Bainaimiao arc. The volcanic rocks have $\epsilon_{\text{Nd}}(t)$ values of +2.11 to +3.77 and zircon $\epsilon_{\text{Hf}}(t)$ values of +5.90 to +11.73, falling between the chondritic and depleted mantle evolution lines (Figure 7a,b), suggesting that their source mainly originated from depleted mantle; the decoupling of $\epsilon_{\text{Nd}}(t)$ and $\epsilon_{\text{Hf}}(t)$ indicates crustal contamination. The Nd isotope T_{DM2} ranges from 823 to 956 Ma, and the Hf isotope T_{DM2} ranges from 636.0 to 1001.4 Ma, representing the mixing ages of juvenile crust and Proterozoic crust, indicating the presence of a Proterozoic crystalline basement in the study area. These characteristics indicate that the Middle Devonian volcanic rocks primarily originated from depleted mantle magmas metasomatized by subduction fluids, with the addition of crustal materials or subducted sediments during their formation.

5.3. Tectonic Setting

In the study area, the Middle–Late Silurian magmatic rocks are mainly composed of basalt, andesite, tonalite, granodiorite, dacite, and rhyolite, which is similar to a typical island arc magmatic rocks assemblage. These rocks are enriched in Rb, Ba, Th, U, and K, while being depleted in Nb, Ta, Sr, P, and Ti, a signature suggesting formation in a subduction zone environment [92,129]. In the Sr/Y vs. Y and La/Yb vs. Th/Yb diagrams (Figure 10a,c), the tonalite and basalt samples fall within the zone of a typical island arc. Additionally, in the Rb vs. (Y + Nb) diagram (Figure 10d), the tonalite samples fall within the zone of a volcanic-arc granite. In the Th/Yb vs. Ta/Yb diagram (Figure 10d), the basalt samples fall within the active continental margin field. These Middle–Late Silurian magmatic rocks (428–419 Ma) share isotopic and geochemical traits with the earlier Late Ordovician to Early Silurian tonalite and quartz diorite (446 Ma, 438 Ma) [29,32]. Notably, the tonalite, characterized by low Sr and high Yb, formed at a depth similar to standard crustal thickness of about 30–40 km [130], suggesting that no arc-continent collision occurred during this period. Therefore, this study suggests that the Middle–Late Silurian magmatic rocks formed in an active continental margin environment.

The Middle Devonian volcanic rocks are marked by low SiO_2 , Na_2O , MgO , Sr , and Y but are rich in K_2O . In the Sr/Y vs. Y diagram (Figure 10a), these samples fall within the zone of the typical island arc. In the Th/Yb vs. Ta/Yb diagram (Figure 10d), the samples fall within the active continental margin field, exhibiting characteristics of the calc-alkaline to shoshonitic series. The La/Yb vs. Th/Yb diagram (Figure 10c) further underscores their affinity with a mature continental arc. Furthermore, the Early Devonian rhyolitic tuff (404 ± 4.5 Ma) in the study area, showing the features of typical A2-type granite, formed in a post-collisional extension setting [29]. In the La/Sm vs. Sm/Yb diagram (Figure 11), the Middle Silurian and Middle Devonian volcanic rock samples can be derived from spinel-garnet lherzolite (Figure 11), with degrees of partial melting ranging from 1 to 5%, and magma source depths estimated between 60 and 80 km [131]. The Middle Silurian volcanic rocks can be derived from spinel lherzolite, whereas the Middle Devonian rocks are more likely derived from spinel-garnet lherzolite (spinel:garnet = 1:1), suggesting an increase in crustal thickness during the Middle Devonian. The collision of the Late Silurian Bainaimiao arc with the NCC led to the subsequent formation of a series of alkaline series magmatic rocks [31,86,132–138]. Combined with the Middle Devonian magmatic rocks in the northern Liaoning Province to central Jiling Province having characteristics of I- and A-type granites [43], this suggests that the study area was an extensional environment after the arc-continent collision during the Middle Devonian period.

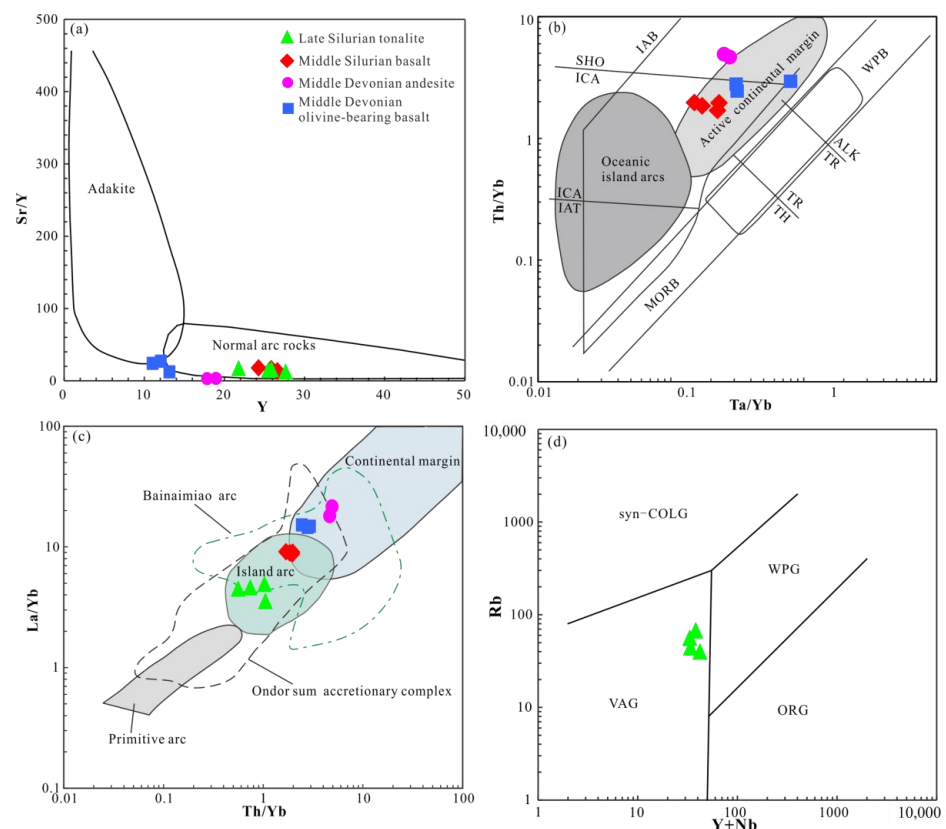


Figure 10. Tectonic environment discriminant diagrams for the Middle Silurian–Middle Devonian magmatic rocks in the Yitong area. (a) Sr/Y versus Sr diagram [139]; (b) Th/Yb versus Ta/Yb diagram [81]; (c) La/Yb versus Th/Yb diagram [140]; (d) Rb versus $(\text{Y} + \text{Nb})$ diagram [141]. MORB: mid-ocean ridge basalts; N-MORB: normal MORB; E-MORB: enriched MORB; WPB: within-plate basalt; OIB: ocean island basalts; OIT: ocean island tholeiitic; OIA: ocean island alkaline; SHO: shoshonite; CAB: calc-alkaline basalts; ICA: island-arc calc-alkaline basalts; IAT: island-arc tholeiitic; IAB: island-arc alkaline basalts; VAG: volcanic-arc granite; Syn-COLG: syn-collision granite; WPG: within plate granite; ORG: ocean-ridge granite.

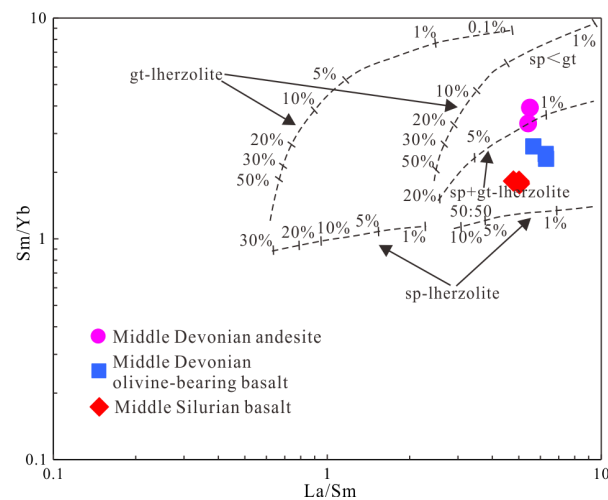


Figure 11. La/Sm-Sm/Yb diagram [141,142] for the Middle Silurian and Middle Devonian magmatic rocks in the Yitong area.

5.4. Silurian–Devonian Tectonic–Magmatic Evolution in the Eastern Section of the Northern Margin of the NCC

Based on previous studies and the division of tectonic evolution, the magmatic and tectonic progression of the eastern section of the northern margin of the NCC from the Silurian to Devonian can be delineated into four primary stages:

5.4.1. Active Continental Margin (443–419 Ma)

Early Paleozoic magmatism along the eastern segment of the northern margin of the NCC commenced in the Late Cambrian and persisted through the Late Silurian. The rock assemblages and peak ages of this Early Paleozoic magmatism align closely with those observed in the central-western segment of the northern margin of the NCC, indicating that the eastern magmatism is a continuation of the Bainaimiao arc [29,32]. Between the Late Cambrian and Middle Ordovician (493–458 Ma), the magmatic rocks are mainly composed of peridotite, pyroxenite, gabbro, high-Mg andesite, pyroxene andesite, quartz diorites, etc., representing the initial stages of subduction [43] within an intra-oceanic arc environment [57], and can be compared with the Ondor Sum subduction-accretionary complex. These early magmatic rocks are primarily located around areas such as Xiaosuhe, Zhangjiatun, Toudaogou, and Huadian, positioned northeastern of the study area, closer to the Changchun Yanji suture zone. Subsequent magmatism (446–419 Ma) is mainly composed of adakitic diorite, andesite, quartz diorites, granodiorites, tonalites, rhyolitic dacites, granites, and rhyolites. These rocks are similar to active continental margin rock assemblages and belong to the calc-alkaline to high-K calc-alkaline series, displaying mature island arc rock characteristics [43]. Silurian magmatic rocks are enriched in LREEs and LILEs, yet are depleted in HFSEs such as Nb, Ta, and Ti, mirroring the geochemistry of arc volcanic rocks. Discrimination diagrams suggest that these Silurian magmatic rocks were produced within an active continental margin setting. Due to subsequent strong modification, rocks from the Late Cambrian and Middle Ordovician are limited and scattered in exposure. Therefore, the position of the immature arc of the Late Cambrian and Middle Ordovician is not very clear. In general, the immature arc of the Late Cambrian and Middle Ordovician is located on the northeast side of the volcanic arc with an age of 446–419 Ma. They can be compared with the Bainaimiao Arc and Ondor Sum subduction-accretionary complex.

South of the Changchun-Yanji Suture zone, the study area records a continuous evolution process from the Late Ordovician to the Permian period. From southwest to northeast, Late Ordovician to Late Silurian intrusive rocks, Silurian to Devonian volcanic and clastic rocks, Late Carboniferous to Early Permian carbonate and clastic rocks, and

Permian metamorphic volcanic rocks are exposed sequentially. Based on rock assemblages, protolith formation, and geochemical characteristics, they can be divided into a Late Ordovician to Late Devonian arc-basin system and a Late Carboniferous to Late Permian arc-basin system. The Paleozoic geological bodies in the area are generally distributed in a northwest direction, and geological bodies of different ages are mostly in tectonic contact, reflecting the process of transpression during the southward subduction of the PAO. In summary, we suggest that the Silurian magmatic rocks in the area formed in an active continental margin environment during the southward subduction of the PAO.

5.4.2. Arc-Continent Collision (419–405 Ma)

The northern margin of the NCC and the Bainaimiao arc show different evolutionary histories and basement properties during the Early Paleozoic era [86]. Currently, many workers believe that the NCC and the Bainaimiao arc underwent an arc-continent collision at the end of the Early Paleozoic and the beginning of the Late Paleozoic [32,42–48]. The Xibiehe Formation and Zhangjiatun Formation, exposed in central Inner Mongolia to central Jilin Province, are considered to be post-collision molasse, unconformably overlying Early Paleozoic units [143]. The Xibiehe Formation in the Jiefangyingzi area of Chifeng City was deposited in the Early Devonian (with tuff interlayer ages of 405 ± 2 Ma); the Zhangjiatun Formation in central Jilin Province was deposited after 404 ± 14 Ma and 409 ± 8 Ma [43]. Detrital zircon geochronology from the Xibiehe Formation indicates that the arc-continent collision occurred during the Late Silurian to the Early Devonian [86]. Moreover, along the Chifeng-Kaiyuan fault, syn-collisional magmatic rocks have been dated to between 419 and 411 Ma [13,15,144,145]. Therefore, the arc-continent collision should have occurred in the Early Devonian (419–405 Ma).

5.4.3. Post-Collisional Extension (404–375 Ma)

During the Devonian period, the northern margin of the NCC and the central to the western section of the Bainaimiao arc show the development of an alkaline magmatic belt from 400 to 380 Ma [31], comprising mafic-ultramafic rocks, alkaline rocks, A-type granites, and bimodal volcanic rocks [31,62,133,135,137,146,147]. These features suggest that this region was in an extensional tectonic environment during the Devonian period. Devonian magmatism in the eastern section of the northern margin of the NCC (414–375 Ma) is mainly composed of basalt, basaltic andesite, andesite, granodiorite, monzonite, dacite, rhyolite, and rhyolite tuff, with notable magmatic peaks at 411 Ma, 400 Ma, 387 Ma, and 377 Ma (Figure 8). Age peaks correspond closely to those in the northern margin of NCC and the Bainaimiao arc (400 Ma, 392 Ma, 379 Ma) [31], suggesting a similar evolutionary history from the eastern to western sections of the northern margin of the NCC during the Devonian period.

In the study area, the Early Devonian rhyolitic tuff (404 Ma) shows A2-type granite geochemical characteristics and was formed in a post-collisional extensional tectonic setting [29]. The Early Devonian monzogranite (400 Ma) and Middle Devonian rhyolite (390 Ma) display adakitic geochemical characteristics, reflecting the thickening of the crust after collision [43,44]. In the Chifeng area, the Middle Devonian syenogranite (392 Ma), granite (385 Ma), and granitic porphyry (377 Ma) [132,148] are classified as A2-type granites, formed in a post-collisional or post-orogenic environment, indicating that the Middle Devonian setting was post-collisional. The intermediate and mafic volcanic rocks from the Middle Devonian (388–384 Ma) in the study area are rich in alkali elements and belong to the shoshonitic series, formed in an extensional setting. In summary, the northern margin of the NCC appears to have been in a post-collisional extensional environment during the Early to Middle Devonian (404–375 Ma).

5.4.4. Active Continental Margin (375–360 Ma)

Previous research suggests that extension during this period may have continued until the end of the Devonian period [70,147–149] or the Early Carboniferous period [150].

Studies on ophiolites and volcanic rocks indicate that southward subduction of the PAO commenced in the Late Devonian to Early Carboniferous. The discovery of Late Devonian calc-alkaline I-type rhyolite in the Yitong area (375.5 ± 4.6 Ma) [29] and high-K calc-alkaline I-type granite in the Changtu area (377 ± 2 Ma) [70] suggests that the PAO plate began to subduct southward during the Late Devonian. Late Devonian high-Mg andesite (370 Ma) in the Faku area, formed in a back-arc rift environment, supports that the PAO underwent southward subduction at this time, leading to the initiation of continental rifting in the Faku area and the development of a post-arc basin [71]. Song et al. [151] based on ophiolites exposed in the CAOB, proposed the existence of two major oceanic expansion/subduction cycles between 500–410 Ma and 360–220 Ma. Xie et al. [152] suggested that the Heishan mafic-ultramafic intrusive rock (357 ± 4 Ma) along the northern margin of the Tarim Craton formed in an active continental margin setting. In summary, this paper posits that the PAO began southward subduction during the Late Devonian (377–360 Ma), leading to the formation of a post-arc basin.

6. Conclusions

(1) Zircon U-Pb dating results show that the Ximangzhang tonalite formed in the Late Silurian (425 ± 6 Ma), while basalt, andesite, and metamorphic olivine-bearing basalt in the Fangniugou volcanic rocks formed in the Middle Silurian (428 ± 6.6 Ma) and Middle Devonian (388.4 ± 3.9 Ma, and 384.1 ± 4.9 Ma, respectively).

(2) The Late Silurian tonalites are characterized by high SiO_2 and Na_2O and low K_2O , MgO , FeOT , and TiO_2 , with an A/CNK ratio of 0.91–1.00, and thus belong to the calc-alkaline series, identified as I-type granite. They are enriched in Rb, Ba, Th, U, and K and depleted in Nb, Sr, P, and Ti, with positive $\varepsilon_{\text{Nd}}(t)$ (+0.35) and $\varepsilon_{\text{Hf}}(t)$ (+0.44 to +6.31) values, suggesting that they mainly originated from partial melting of Meso–Neoproterozoic era accretionary lower crustal material (basalt). The Middle Silurian basalts are characterized by low SiO_2 , P_2O_5 , TiO_2 , and Na_2O and high Al_2O_3 , FeOT , and K_2O , enriched in Rb, Ba, Th, U, and K and depleted in Nb, Ta, Sr, P, and Ti, indicative of shoshonitic basalt. The Late Silurian tonalite has positive $\varepsilon_{\text{Nd}}(t)$ (+4.91 to +6.18) values and primarily originated from depleted mantle magmas metasomatized by subduction fluids, supplemented by a small amount of subducted sediments and crustal materials. The Middle–Late Silurian magmatic rocks formed in an active continental margin environment influenced by the southward subduction of the PAO.

(3) The Middle Devonian volcanic rocks exhibit low SiO_2 , TiO_2 , and Na_2O and high K_2O , and MgO and enriched in Rb, K, and LREEs and depleted in Nb, Ta, Sr, and HREEs, characteristic of shoshonitic volcanic rocks. $\varepsilon_{\text{Nd}}(t)$ (+2.11 to +3.77) and $\varepsilon_{\text{Hf}}(t)$ (+5.90 to +11.73) values are positive. These characteristics suggest that the Middle Devonian volcanic rocks primarily originated from depleted mantle magmas metasomatized by subduction fluids, with the addition of crustal materials or subducted sediments during their formation. The Middle Devonian magmatic rocks formed in an extensional environment after the arc-continent collision.

Supplementary Materials: The following supporting information can be downloaded at: <https://www.mdpi.com/article/10.3390/min14070641/s1>, Table S1. LA-ICP-MS zircon U-Pb data of samples from the Yitong Area; Table S2. Major element (wt.%), and trace elements (ppm) compositions of samples from the Yitong Area; Table S3. Lu-Hf isotopic compositions of zircons from the Yitong area; Table S4. Sr-Nd isotopic compositions of samples from the Yitong area.

Author Contributions: Methodology, B.L.; Investigation, B.L., F.Y., M.L., Y.Z. and C.Z.; Data curation, B.L.; Writing—original draft, B.L. and J.C., Writing—review & editing, B.L. and J.C. All authors have read and agreed to the published version of the manuscript.

Funding: This research was funded by the China Geological Survey (Grants DD20242929, DD20230210, and DD20190042-04) and the funding project of Northeast Geological S&T Innovation Center of China Geological Survey (NO. QCJJ2022–42).

Data Availability Statement: The authors confirm that the data generated or analyzed during this study are provided in full within the published article.

Conflicts of Interest: The authors declare no conflict of interest.

References

1. Badarch, G.; Cunningham, W.D.; Windley, B.F. A new terrane subdivision for Mongolia: Implications for the Phanerozoic crustal growth of central Asia. *J. Asian Earth Sci.* **2002**, *21*, 87–110. [[CrossRef](#)]
2. Buslov, M.M.; Saphonova, I.Y.; Watanabe, T.; Obut, O.T.; Fujiwara, Y.; Iwata, K.; Semakov, N.N.; Sugai, Y.; Smirnova, L.V.; Kazansky, A.Y. Evolution of the Paleo-Asian Ocean (Altai-Sayan region, central Asia) and collision of possible Gondwana-derived terranes with the southern marginal part of the Siberian continent. *Geosci. J.* **2001**, *5*, 203–224. [[CrossRef](#)]
3. Xiao, W.J.; Huang, B.C.; Han, C.M.; Sun, S.; Li, J.L. A review of the western part of the Altaids: A key to understanding the architecture of accretionary orogens. *Gondwana Res.* **2010**, *18*, 253–273. [[CrossRef](#)]
4. Xiao, W.J.; Windley, B.F.; Sun, S.; Li, J.L.; Huang, B.C.; Han, C.M.; Yuan, C.; Sun, M.; Chen, H.L. A tale of amalgamation of three Permo-Triassic Collage Systems in Central Asia: Oroclines, sutures, and terminal accretion. *Annu. Rev. Earth Planet. Sci.* **2015**, *43*, 477–507. [[CrossRef](#)]
5. Xu, B.; Zhao, P.; Wang, Y.Y.; Liao, W.; Luo, Z.W.; Bao, Q.Z.; Zhou, Y.H. The Pre-Devonian tectonic framework of Xing’an-Mongolia orogenic belt (XMOB) in North China. *J. Asian Earth Sci.* **2015**, *97*, 183–196. [[CrossRef](#)]
6. Liu, Y.J.; Li, W.M.; Feng, Z.Q.; Wen, Q.B.; Neubauer, F.; Liang, C.Y. A review of the Paleozoic tectonics in the eastern part of Central Asian Orogenic Belt. *Gondwana Res.* **2017**, *43*, 123–148. [[CrossRef](#)]
7. Windley, B.F.; Allen, M.B.; Zhang, C.; Zhao, Z.Y.; Wang, G.R. Paleozoic accretion and Cenozoic redeformation of the Chinese Tien Shan Range. *Cent. Asia Geol.* **1990**, *18*, 128–131.
8. Sengör, A.M.C.; Natal’in, B.A.; Burtman, V.S. Evolution of the Altaid tectonic collage and Paleozoic crustal growth in Eurasia. *Nature* **1993**, *364*, 299–307. [[CrossRef](#)]
9. Yakubchuk, A. Architecture and mineral deposit settings of the Altaid orogenic collage: A revised model. *J. Asian Earth Sci.* **2004**, *23*, 761–779. [[CrossRef](#)]
10. Jahn, B.M.; Wu, F.Y.; Hong, D.W. Important crustal growth in the Phanerozoic: Isotopic evidence of granitoids from East central Asia. *J. Earth Syst. Sci.* **2000**, *109*, 5–20. [[CrossRef](#)]
11. Liu, Y.J.; Li, W.M.; Ma, Y.F.; Feng, Z.Q.; Guan, Q.B.; Li, S.Z.; Chen, Z.X.; Liang, C.Y.; Wen, Q.B. An orocline in the eastern Central Asian Orogenic Belt. *Earth-Sci. Rev.* **2021**, *221*, 103808. [[CrossRef](#)]
12. Wu, F.Y.; De, Y.S.; Wen, C.G.; Zhang, Y.B.; Grant, M.L.; Wilde, S.A.; Jahn, B.M. Geochronology of the Phanerozoic granitoids in northeastern China. *J. Asian Earth Sci.* **2011**, *41*, 1–30. [[CrossRef](#)]
13. Jian, P.; Liu, D.Y.; Krner, A.; Windley, B.F.; Shi, Y.R.; Zhang, F.Q.; Shi, G.H.; Miao, L.C.; Zhang, W.; Zhang, Q.; et al. Time scale of an Early to Mid-Paleozoic orogenic cycle of the long-lived Central Asian Orogenic Belt, Inner Mongolia of China: Implications for continental growth. *Lithos* **2008**, *101*, 233–259. [[CrossRef](#)]
14. Xu, B.; Zhao, P.; Bao, Q.Z.; Zhou, Y.H.; Wang, Y.Y.; Luo, Z.W. Preliminary study on the Pre-Mesozoic tectonic unit division of the Xing-Meng Orogenic Belt (XMOB). *Acta Petrol. Sin.* **2014**, *30*, 1841–1857.
15. Chen, J.S.; Liu, M.; Li, B.; Li, W.; Li, W.W.; Yang, F.; Wang, Y. Zircon U-Pb chronology and geochemical characteristics of Late Silurian monzogranite in Ongniud Banner, Inner Mongolia. *Geol. Bull. China* **2017**, *36*, 1359–1368. (In Chinese with English Abstract)
16. Feng, Z.Q.; Liu, Y.J.; Li, L.; Jin, W.; Jiang, L.W.; Li, W.M.; Wen, Q.B.; Zhao, Y.L. Geochemical and geochronological constraints on the tectonic setting of the xinlin ophiolite, northern Great Xing’an Range, NE China. *Lithos* **2019**, *326–327*, 213–229. [[CrossRef](#)]
17. Liu, Y.J.; Feng, Z.Q.; Jiang, L.W.; Jin, W.; Li, W.M.; Guan, Q.B.; Wen, Q.B.; Liang, C.Y. Ophiolite in the eastern Central Asian Orogenic Belt, NE China. *Acta Petrol. Sin.* **2019**, *35*, 3017–3047. (In Chinese with English Abstract)
18. Wu, F.Y.; Jahn, B.M.; Wilde, S.M.; Sun, D.Y. Phanerozoic crustal growth: U-Pb and Sr-Nd isotopic evidence from the granites in northeastern China. *Tectonophysics* **2000**, *328*, 89–113. [[CrossRef](#)]
19. Wu, F.Y.; Li, X.H.; Yang, J.H.; Zheng, Y.F. Discussions on the petrogenesis of granites. *Acta Petrol. Sin.* **2007**, *23*, 1217–1238. (In Chinese with English Abstract)
20. Xiao, W.J.; Windley, B.F.; Hao, J.; Zhai, M.G. Accretion leading to collision and the Permian Solonker suture, Inner Mongolia, China: Termination of the Central Asian Orogenic Belt. *Tectonics* **2003**, *22*, 1069. [[CrossRef](#)]
21. Xiao, W.J.; Krner, A.; Windley, B.F. Geodynamic evolution of Central Asia in the Paleozoic and Mesozoic. *Int. J. Earth Sci.* **2009**, *98*, 1185–1188. [[CrossRef](#)]
22. Li, J.Y. Permian geodynamic setting of Northeast China and adjacent regions: Closure of the Paleo-Asian Ocean and subduction of the Paleo-Pacific Plate. *J. Asian Earth Sci.* **2006**, *26*, 207–224. [[CrossRef](#)]
23. Jian, P.; Liu, D.Y.; Kröner, A.; Windley, B.F.; Shi, Y.R.; Zhang, W.; Zhang, F.Q.; Miao, L.C.; Zhang, L.Q.; Tomurhuu, D. Evolution of a Permian intraoceanic arc-trench system in the solonker suture zone, Central Asian Orogenic Belt, China and Mongolia. *Lithos* **2010**, *118*, 169–190. [[CrossRef](#)]
24. Wilde, S.A. Final amalgamation of the Central Asian Orogenic Belt in NE China: Paleo-Asian Ocean closure versus Paleo-Pacific plate subduction: A review of the evidence. *Tectonophysics* **2015**, *662*, 345–362. [[CrossRef](#)]

25. Chen, J.S.; Tian, D.X.; Yang, H.; Li, W.W.; Liu, M.; Li, B.; Yang, F.; Li, W.; Wu, Z. Triassic granitic magmatism at the northern margin of the North China Craton: Geochronology, geochemistry, and implications for the tectonic evolution of the Central Asian Orogenic Belt. *Acta Geol. Sin. (Engl. Ed.)* **2019**, *93*, 1325–1353. [[CrossRef](#)]
26. Zhang, C.; Neubauer, F.; Liu, Z.H.; Cui, F.H.; Guan, Q.B. Final-stage magmatic record of Paleo-Asian Oceanic subduction? Insights from Late Permian to Early Triassic intrusive rocks in the Yanbian area, easternmost Central Asian Orogenic Belt. *Minerals* **2020**, *10*, 799. [[CrossRef](#)]
27. Guan, Q.B.; Liu, Z.H.; Liu, Y.J.; Li, S.Z.; Wang, S.J.; Chen, Z.X.; Zhang, C. A tectonic transition from closure of the Paleo-Asian Ocean to subduction of the Paleo-Pacific plate: Insights from Early Mesozoic igneous rocks in eastern Jilin Province, NE China. *Gondwana Res.* **2022**, *102*, 332–353. [[CrossRef](#)]
28. Yang, H.; Ge, W.C.; Santosh, M.; Ji, Z.; Dong, Y.; Jing, Y.; Wu, H.R. The role of continental fragments in the formation of intra-oceanic arcs: Constraints from Sr-Nd-Hf-O isotopes of gabbro from the Jiamusi Block, NE China. *Gondwana Res.* **2022**, *103*, 297–313. [[CrossRef](#)]
29. Li, B.; Shi, Y.; Yang, F.; Liu, M.; Wu, Z. Middle Silurian-Late Devonian tectonic evolution in the eastern segment of the northern margin of the North China Plate: Evidence from magmatic rocks in Gongzhuling area. *Acta Petrol. Sin.* **2022**, *38*, 2364–2396. (In Chinese with English Abstract)
30. Shi, G.Z.; Faure, M.; Xu, B.; Zhao, P.; Chen, Y. Structural and kinematic analysis of the Early Paleozoic Ondor Sum-Hongqi mélangé belt, eastern part of the Altaids (CAOB) in Inner Mongolia, China. *J. Asian Earth Sci.* **2013**, *66*, 123–139. [[CrossRef](#)]
31. Zhang, Q.Q.; Zhang, S.H.; Zhao, Y.; Liu, J.M. Devonian alkaline magmatic belt along the northern margin of the North China Block: Petrogenesis and tectonic implications. *Lithos* **2018**, *302*, 496–518. [[CrossRef](#)]
32. Zhang, S.H.; Zhao, Y.; Ye, H.; Liu, J.M.; Hu, Z.C. Origin and evolution of the Bainaimiao arc belt: Implications for crustal growth in the southern Central Asian Orogenic Belt. *Geol. Soc. Am. Bull.* **2014**, *126*, 1275–1300. [[CrossRef](#)]
33. Zhou, Z.H.; Mao, J.W.; Ma, X.H.; Che, H.W.; Ouyang, H.G.; Gao, X. Geochronological framework of the Early Paleozoic Bainaimiao Cu-Mo-Au deposit, NE China, and its tectonic implications. *J. Asian Earth Sci.* **2017**, *144*, 323–338. [[CrossRef](#)]
34. Qian, C.; Lu, L.; Wang, Y.; Guo, R.R.; Tang, Z. Age and geochemistry of amphibolite in Shuangsheng area, eastern Inner Mongolia: New evidence from the Paleoproterozoic basement of Bainaimiao island arc. *Geol. Bull. China* **2020**, *39*, 905–918. (In Chinese with English Abstract)
35. Chen, Y.; Zhang, Z.; Qian, X.; Li, J.; Ji, Z.; Wu, T. Early to Mid-Paleozoic magmatic and sedimentary records in the Bainaimiao Arc: An advancing subduction-induced terrane accretion along the northern margin of the North China Craton. *Gondwana Res.* **2020**, *79*, 263–282. [[CrossRef](#)]
36. Zhou, Z.G.; Zhang, D.; Gu, Y.C.; Wang, G.S.; Li, Y.H.; Yu, Y.S.; Liu, C.F.; Liu, W.C. Characteristics of Bainaimiao thrust belt along central Inner Mongolia in North China and its geological significance. *Geotecton. Metallog.* **2018**, *42*, 1–17. (In Chinese with English Abstract)
37. Gao, J.Y.; Wang, Y.X.; Qiu, Y.Z.; Zhang, Q. Islands-ocean structural evolution of mid-western continent in Inner Mongolia. *Geotecton. Metallog.* **2001**, *25*, 397–404. (In Chinese with English Abstract)
38. Shang, H.S.; Tao, J.X.; Baoyin, W.L.J.; Hao, X.Y. The arc-basin system and tectonic significance of Early Paleozoic in Baiyun'ebo area Inner Mongolia. *Geol. Surv. Res.* **2003**, *26*, 160–168 (In Chinese with English Abstract)
39. De Jong, K.; Xiao, W.J.; Windley, B.F.; Masago, H.; Lo, C.H. Ordovician ⁴⁰Ar/³⁹Ar phengite ages from the blueschist-facies OndorSum subduction-accretion complex (Inner Mongolia) and implications for the Early Paleozoic history of continental blocks in China and adjacent areas. *Am. J. Sci.* **2006**, *306*, 799–845. [[CrossRef](#)]
40. Xu, B.; Charvet, J.; Chen, Y.; Zhao, P.; Shi, G. Middle Paleozoic convergent orogenic belts in western Inner Mongolia (China): Framework, kinematics, geochronology and implications for tectonic evolution of the Central Asian Orogenic Belt. *Gondwana Res.* **2013**, *23*, 1342–1364. [[CrossRef](#)]
41. Wu, C.; Liu, C.F.; Zhu, Y.; Zhou, Z.G.; Jiang, T.; Liu, W.C.; Li, H.Y.; Wu, C.; Ye, B.Y. Early Paleozoic magmatic history of central Inner Mongolia, China: Implications for the tectonic evolution of the southeast Central Asian Orogenic Belt. *Int. J. Earth Sci.* **2016**, *105*, 1307–1327. [[CrossRef](#)]
42. Ma, S.X.; Wang, Z.; Zhang, Y.; Sun, J. Bainaimiao arc as an exotic terrane along the northern margin of the north china craton: Evidences from petrography, zircon U-Pb dating, and geochemistry of the Early Devonian deposits. *Tectonics* **2019**, *38*, 2606–2624. [[CrossRef](#)]
43. Pei, F.P.; Zhang, Y.; Wang, Z.W.; Cao, H.H.; Xu, W.L.; Wang, Z.J.; Wang, F.; Yang, C. Early-Middle Paleozoic subduction-collision history of the south-eastern Central Asian Orogenic Belt: Evidence from igneous and metasedimentary rocks of central Jilin Province, NE China. *Lithos* **2016**, *261*, 164–180. [[CrossRef](#)]
44. Han, Z.Z.; Song, Z.G.; Han, C.; Zhong, W.J.; Han, M.; Yan, J.L.; Liu, H.; Du, Q.X.; Gao, L.H.; Li, J.J. U-Pb ages and Hf isotopic composition of zircons and whole rock geochemistry of volcanic rocks from the Fangniugou area: Implications for Early–Middle Paleozoic tectonic evolution in Jilin Province, NE China. *J. Miner. Petrol. Sci.* **2018**, *113*, 10–23. [[CrossRef](#)]
45. Song, Z.G.; Han, C.; Liu, H.; Han, Z.Z.; Yan, J.L.; Zhong, W.J.; Gao, L.H.; Du, Q.X.; Han, M.; Li, J.J. Early-Middle Ordovician intermediate-mafic and ultramafic rocks in central Jilin Province, NE China: Geochronology, origin, and tectonic implications. *Min. Petrol.* **2019**, *113*, 393–415. [[CrossRef](#)]
46. Chen, Q.; Chou, G.L.; Xue, L.F.; Zhou, X.M.; Zhou, H.P.; Du, Y.S. Palaeoplate evolution in the southern part of the Inner Mongolian orogenic belt. *Geol. Rev.* **1993**, *39*, 477–483. (In Chinese with English Abstract)

47. Li, S.Q. Early Palaeozoic era of terrane pieced together and accreted in middle of Inner Mongolia. *Geol. Inn. Mong.* **1997**, *1*, 18–230. (In Chinese with English Abstract)
48. Wang, Z.W.; Pei, F.P.; Xu, W.L.; Cao, H.H.; Wang, Z.J.; Zhang, Y. Tectonic evolution of the eastern Central Asian Orogenic Belt: Evidence from zircon U-Pb-Hf isotopes and geochemistry of Early Paleozoic rocks in Yanbian region, NE China. *Gondwana Res.* **2016**, *38*, 334–350. [[CrossRef](#)]
49. Tang, K.D. *Tectonic Evolution and Minerogenetic Regularities of the Fold Belt along the Northern Margins of Sino-Korean Plate*; Peking University Press: Beijing, China, 1992; pp. 1–285. (In Chinese)
50. Hu, X.; Xu, C.S.; Niu, S.Y. *Continental Edge Evolution of Early Paleozoic Era in the Northern Margin of Huabei Platform*; Peking University Press: Beijing, China, 1990; pp. 1–273. (In Chinese with English Abstract)
51. Zhang, C.; Liu, Y.J.; Zhang, Z.L.; Cui, F.H.; Guan, Q.B.; Li, Y. Deformation and geochronological characteristics of Gudonghe ductile shear zone in Yanbian area. *Earth Sci.* **2019**, *44*, 3252–3264. (In Chinese with English Abstract)
52. Li, J.W.; Pei, R.F.; Zhang, D.Q.; Wang, C.X.; Po, Y.H. Metallogenic geological evolution of Bainaimiao copper deposit, Inner Mongolia. *Miner. Depos.* **2002**, *21*, 405–408. (In Chinese)
53. Nie, F.J.; Zhang, H.T.; Chen, Q.; Meng, L.Y.; Qiu, G.L.; Li, D.L. The zircon U-Pb age of metamorphosed basic volcanic rocks from the Bainaimiao Group in Inner Mongolia. *Chin. Sci. Bull.* **1991**, *36*, 738–742.
54. Li, J.J.; Dang, Z.C.; Zhao, Z.L.; Shi, Y.R.; Liu, D.Y.; Li, C.; Qu, W.J.; Wang, C.X.; Fu, C.; Tang, W.L.; et al. The metallogenic epochs of Bainaimiao copper deposit in Inner Mongolia. *Acta Geol. Sin.* **2015**, *89*, 1448–1457. (In Chinese with English Abstract)
55. Zhao, L.G.; Li, C.D.; Chang, Q.S.; Gao, X.S.; Xu, Y.W.; Fan, J.T.; Zhang, K.A. Tentative discussion on zircon U-Pb geochronology and geochemistry of ore-bearing intermediate-acid intrusive rocks in the Bainaimiao copper ore district and the metallogenic epoch. *Geol. Bull. China* **2016**, *35*, 542–552. (In Chinese with English Abstract)
56. Pei, F.P.; Wang, Z.W.; Cao, H.H.; Xu, W.L.; Wang, F. Petrogenesis of the Early Paleozoic tonalite in the central Jilin Province: Evidence from zircon U-Pb chronology and geochemistry. *Acta Petrol. Sin.* **2014**, *30*, 2009–2019. (In Chinese with English Abstract)
57. Ma, H.T.; Ma, X.; Chen, J.F.; Chen, B.; Li, C.; Zhou, L.M.; Yang, H.Z. The Zhangjiatun igneous complex in the southeastern margin of the Central Asian Orogenic Belt, NE China: Evidence for an Early Paleozoic intra-oceanic arc. *J. Asian Earth Sci.* **2020**, *194*, 104182. [[CrossRef](#)]
58. Jia, D.C.; Hu, R.Z.; Lu, Y.; Qiu, X.L. Collision belt between the Khanka block and the North China block in the Yanbian region, Northeast China. *J. Asian Earth Sci.* **2004**, *23*, 211–219.
59. Zhang, Y.B.; Wu, F.; Wilde, S.A.; Zhai, M.; Lu, X.; Sun, D. Zircon U-Pb ages and tectonic implications of “Early Paleozoic” granitoids at Yanbian, Jilin Province, Northeast China. *Isl. Arc* **2004**, *13*, 484–505. [[CrossRef](#)]
60. Tang, K.D.; Shao, J.A.; Li, J.C.; Kang, Z. Nature of the Yanbian suture zone and structure of Northeast Asia. *Geol. Bull. China* **2004**, *23*, 885–891. (In Chinese with English Abstract)
61. Li, C.D.; Zhang, F.Q.; Miao, L.C.; Xie, H.Q.; Xu, Y.W. Zircon SHRIMP geochronology and geochemistry of Late Permian high-Mg andesites in Seluohe area, Jilin province, China. *Acta Petrol. Sin.* **2007**, *23*, 767–776. (In Chinese with English Abstract)
62. Zhang, C.Y. Tectonic Implication of Paleozoic Metamorphic Complexes in East Jilin. Ph.D. Thesis, Jilin University, Changchun, China, 2009. (In Chinese with English Abstract)
63. Zhang, C. The Mesozoic Tectonic Evolution of Yanbian Area in the Eastern Segment of Northern Margin of the North China Block. Ph.D. Thesis, Jilin University, Changchun, China, 2014. (In Chinese with English abstract)
64. Wang, Z.W.; Pei, F.P.; Xu, W.L.; Cao, H.H.; Wang, Z.J. Geochronology and geochemistry of Late Devonian and Early Carboniferous igneous rocks of central Jilin Province, NE China: Implications for the tectonic evolution of the eastern Central Asian Orogenic Belt. *J. Asian Earth Sci.* **2015**, *97*, 260–278. [[CrossRef](#)]
65. Zhao, C.; Gong, E.P.; Liu, J.; Song, S.E.; Peng, Y.B.; Cui, Y.S. Disintegration and reunderstanding of the “Kaiyuan rock group” in the east section of the northern margin of North China Craton. *Geol. Resour.* **2018**, *27*, 209–217. (In Chinese with English Abstract)
66. Zhou, J.B.; Cao, J.L.; Han, W.; Li, G.Y. The Changchun-Yanji suture zone: Nature and tectonic implications. *Acta Petrol. Sin.* **2020**, *36*, 636–643. (In Chinese with English Abstract)
67. Zhang, X.Z.; Ma, Y.X.; Chi, X.G.; Zhang, F.X.; Sun, Y.W.; Guo, Y.; Zeng, Z. Discussion on Phanerozoic tectonic evolution in Northeastern China. *J. Jilin Univ. (Earth Sci. Ed.)* **2012**, *42*, 1269–1285. (In Chinese with English Abstract)
68. Jiang, Z.L.; Qiu, H.J.; Peng, Y.Q.; Zhang, W.M.; Liang, S. Zircon SHRIMP U-Pb dating for island arc volcanic rock of Fangniugou area in Yitong region of Jilin Province. *J. Cent. South Univ.* **2014**, *21*, 2877–2884. [[CrossRef](#)]
69. Han, Z.Z.; Song, Z.G.; Gao, L.H.; Han, M.; Guo, Z.P.; Zhong, W.J.; Li, J.J.; Du, Q.X.; Yan, J.L.; Liu, H. Late Paleozoic volcanic events in “Daheishan Horst” in Jilin, China and their tectonic significance. *Earth Sci. Front.* **2017**, *24*, 186–201. (In Chinese with English Abstract)
70. Zhang, C.; Quan, J.Y.; Zhang, L.; Ge, J.T.; Zhang, L.D. Devonian extension of the eastern section of the northern margin of the North China Plate: Evidence from post-collision magmatic rocks in Changtu area, northern Liaoning Province. *Acta Petrol. Sin.* **2022**, *38*, 2345–2363. (In Chinese with English Abstract)
71. Shi, Y.; Shi, S.S.; Liu, Z.H.; Wang, L.; Liu, J.; Chen, J.S.; Yang, F.; Zhang, C.; Li, B.; Zhang, L.D. Back-arc system formation and extinction in the southern Central Asian Orogenic Belt: New constraints from the Faku ophiolite in north Liaoning, NE China. *Gondwana Res.* **2022**, *103*, 64–83. [[CrossRef](#)]
72. Bureau of Geology and Mineral Resources of Jilin Province(BGMRJ). *Stratigraphy (Lithostratigraphy) of Jilin Province*; China University of Geosciences Press: Wuhan, China, 1997; pp. 1–324. (In Chinese)

73. Wiedenbeck, M.; Allé, P.; Corfu, F.; Griffin, W.L.; Meier, M.; Oberli, F.; Quadt, A.; Roddick, J.C.; Spiegel, W. Three natural zircon standards for U-Th-Pb, Lu-Hf, trace element and REE analyses. *Geostand. Geoanalytical Res.* **1995**, *19*, 1–23. [[CrossRef](#)]
74. Yuan, H.L.; Gao, S.; Liu, X.M.; Li, H.M.; Günther, D.; Wu, F.Y. Accurate U-Pb age and trace element determinations of zircon by laser ablation-inductively coupled plasma mass spectrometry. *Geostand. Geoanalytical Res.* **2004**, *28*, 353–370. [[CrossRef](#)]
75. Geng, J.Z.; Li, H.K.; Zhang, J.; Zhou, H.Y.; Li, H.M. Zircon Hf isotope analysis by means of LA-MC-ICP-MS. *Geol. Bull. China* **2011**, *30*, 1508–1513. (In Chinese with English Abstract)
76. Irber, W. The lanthanide tetrad effect and its correlation with K/Rb, Eu/Eu*, Sr/Eu, Y/Ho, and Zr/Hf of evolving peraluminous granitesuites. *Geochim. Cosmochim. Acta* **1999**, *63*, 489–508. [[CrossRef](#)]
77. Monecke, T.; Kempe, U.; Monecke, J.; Sala, M.; Wolf, D. Tetrad effect in rare earth element distribution patterns: A method of quantification with application to rock and mineral samples from granite-related rare metal deposits. *Geochim. Cosmochim. Acta* **2002**, *66*, 1185–1196. [[CrossRef](#)]
78. O'Connor, J. A classification for quartz-rich igneous rock based on feldspar ratios. *US Geol. Surv. Prof. Pap. B* **1965**, *525*, 79–84.
79. Winchester, J.A.; Floyd, P.A. Geochemical discrimination of different magma series and their differentiation products using immobile elements. *Chem. Geol.* **1977**, *20*, 325–343. [[CrossRef](#)]
80. Peccerillo, R.; Taylor, S.R. Geochemistry of eocene calc-alkaline volcanic rocks from the Kastamonu area, Northern Turkey. *Contrib. Miner. Pet.* **1976**, *58*, 63–81. [[CrossRef](#)]
81. Pearce, J.A. Trace elements characteristic of lavas from destructive plate boundaries. Andesites. In *Orogenic Andesites and Related Rocks*; Thorpe, R.S., Ed.; John Wiley & Sons: Chichester, UK, 1982; pp. 525–548.
82. Moine, B.; De La Roche, H. Nouvelle approche du problème de l'origine des amphibolites à partir de leur composition chimique. *C. R. Acad. Sci. Paris* **1968**, *267*, 2084–2087.
83. Boynton, W.V. Geochemistry of the rare earth elements: Meteorite studies. *Dev. Geochem.* **1984**, *2*, 63–114.
84. Sun, S.S.; McDonough, W.F. Chemical and isotopic systematics of oceanic basalts: Implications for mantle composition and processes. In *Magmatism in Ocean Basins*; Geological Society, London, Special Publication; Sanders, A.D., Norry, M.J., Eds.; Blackwell Scientific Publications: Oxford, UK, 1989; Volume 42, pp. 313–345.
85. Yang, J.H.; Wu, F.Y.; Shao, J.A.; Wilde, S.A.; Xie, L.W.; Liu, X.M. Constraints on the timing of uplift of the Yanshan fold and thrust belt, North China. *Earth Planet. Sci. Lett.* **2006**, *246*, 336–352. [[CrossRef](#)]
86. Zhang, Q.Q. Geological Records of the Late Silurian-Devonian Arc-Continent Collision in the Northern Margin of the North China Block and Craton-Orogen Boundary. Ph.D. Thesis, Chinese Academy of Geological Sciences, Beijing, China, 2021; pp. 1–203. (In Chinese with English Abstract)
87. Shi, Y.; Liu, Z.H.; Liu, Y.J.; Shi, S.S.; Wei, M.H.; Yang, J.J.; Gao, T. Late Paleozoic-Early Mesozoic southward subduction-closure of the Paleo-Asian Ocean: Proof from geochemistry and geochronology of Early Permian-Late Triassic felsic intrusive rocks from North Liaoning, NE China. *Lithos* **2019**, *346*, 105165.
88. Zhao, C.Q.; Zhang, Z.B.; Shi, Y.; Shi, S.S.; You, H.X.; Chen, C.; Zhao, J.Y. The deformation and metamorphic features of Faku metamorphic complex the composition and tectonic affinity in the northern Liaoning Province. *Acta Petrol. Sin.* **2021**, *37*, 1983–2006. (In Chinese with English Abstract)
89. Shi, Y.; Shi, S.S.; Chen, X.; Huan, F.M. The extinction process of the paleo-oceanic basin in the eastern part of the northern margin of the North China Block: Implications from the intermediate-mafic magmatic rocks in the northern Liaoning, NE China. *Acta Petrol. Sin.* **2022**, *38*, 2292–2322. (In Chinese with English Abstract)
90. Guan, Q.B. Permian-Early Jurassic Tectonic Evolution of Kaiyuan-Yanji Area in the Eastern Segment of the Northern Margin of the North China Block. Ph.D. Thesis, Jilin University, Changchun, China, 2018. (In Chinese with English Abstract)
91. Shi, Y.; Chen, J.S.; Wei, M.H.; Shi, S.S.; Zhang, C.; Zhang, L.D.; Hao, Y.J. Evolution of eastern segment of the Paleo-Asian Ocean in the Late Paleozoic: Geochronology and geochemistry constraints of granites in Faku area, North Liaoning, NE China. *Acta Petrol. Sin.* **2020**, *36*, 3287–3308. (In Chinese with English Abstract)
92. Kelemen, P.B.; Rilling, J.L.; Parmentier, E.M.; Mehl, L.; Hacker, B.R. Thermal structure due to solid-state flow in the mantle wedge beneath arcs. *Geophys. Monogr.-Am. Geophys. Union* **2003**, *138*, 293–311.
93. Liu, J.F. Late Paleozoic Magmatism and Its Constraints on Regional Tectonic Evolution in Linxi-Dongwuqi Area, Inner Mongolia. Ph.D. Thesis, Jilin University, Changchun, China, 2009. (In Chinese with English Abstract)
94. McLennan, S.M. Rare earth element geochemistry and the “tetrad” effect. *Geochim. Cosmochim. Acta* **1994**, *58*, 2025–2033. [[CrossRef](#)]
95. Zhao, J.X.; Cooper, J. Fractionation of monazite in the development of V-shaped REE patterns in leucogranite systems: Evidence from amuscovite leucogranite body in central Australia. *Lithos* **1993**, *30*, 23–32. [[CrossRef](#)]
96. Zhao, Z.H.; Musuda, A.; Shabani, M.B. Tetrad effects of rare-earth elements in rare-metal granites. *Geochimica* **1992**, *3*, 221–233. (In Chinese with English Abstract)
97. Bau, M. Controls on the Fractionation of isoivalent trace elements in magmatic and aqueous systems: Evidence from Y/Ho, Zr/Hf, and Lanthanide tetrad effect. *Contrib. Miner. Petrol.* **1996**, *123*, 323–333. [[CrossRef](#)]
98. Ellison, A.J.; Hess, P.C. Solution behavior of 14 cations in high silicamelts: Petrologic and geochemical implications. *Contrib. Miner. Petrol.* **1986**, *94*, 343–351. [[CrossRef](#)]
99. Hu, G.Y.; Zeng, L.S.; Gao, L.E.; Xie, K.J. Lanthanide kinked shape, similar to tetrad effect, observed in sub-volcanic rocks from Qiaga, southern Tibet, China. *Geol. Bull. China* **2011**, *30*, 82–94. (In Chinese with English Abstract)

100. Rapp, R.P.; Watson, E.B. Monazite solubility and dissolution kinetics: Implication for the thorium and light rare earth geochemistry of felsic magmas. *Contrib. Miner. Petrol.* **1986**, *94*, 304–316. [[CrossRef](#)]
101. Lassiter, J.C.; DePaolo, D.J. Plume/lithosphere interaction in the generation of continental and oceanic flood basalts: Chemical and isotopic constraints. In *Large Igneous Provinces: Continental, Oceanic, and Planetary Flood Volcanism*; Mahoney, J.J., Coffin, M.F., Eds.; American Geophysical Union: Washington, DC, USA, 1997; Volume 100, pp. 335–355.
102. Genç, S.C.; Tüysüz, O. Tectonic setting of the Jurassic bimodal magmatism in the Sakarya Zone (Central and Western Pontides), Northern Turkey: A geochemical and isotopic approach. *Lithos* **2010**, *118*, 95–111. [[CrossRef](#)]
103. Collins, W.; Beams, S.; White, A.; Chappell, B.W. Nature and Origin of A-type Granites with Particular Reference to Southeastern Australia. *Contrib. Miner. Petrol.* **1982**, *80*, 189–200. [[CrossRef](#)]
104. Whalen, J.B.; Currie, K.L.; Chappell, B.W. A-type granites: Geochemical characteristics, discrimination and petrogenesis. *Contrib. Miner. Petrol.* **1987**, *95*, 407–419. [[CrossRef](#)]
105. Sylvester, P.J. Post-collisional strongly peraluminous granites. *Lithos* **1998**, *45*, 29–44. [[CrossRef](#)]
106. Taylor, S.R.; McLennan, S. *The Continental Crust: Its Composition and Evolution*; Blackwell Scientific Publications: Boston, MA, USA, 1985; pp. 209–230.
107. Workman, R.K.; Hart, S.R. Major and trace element composition of the depleted MORB mantle (DMM). *Earth Planet. Sci. Lett.* **2005**, *231*, 1–328. [[CrossRef](#)]
108. Menzies, M.A.; Kyle, P.R.; Jones, M.; Ingram, G. Enriched and depleted source components for tholeiitic and alkaline lavas from Zuni-Bandera, New Mexico: Inferences about intraplate processes and stratified lithosphere. *J. Geophys. Res. Solid Earth* **1991**, *96*, 13645–13671. [[CrossRef](#)]
109. Saunders, A.D.; Norry, M.J.; Tarney, J. Fluid influence on the trace element compositions of subduction zone magmas. *Philos. Trans. R. Soc. A Math. Phys. Eng. Sci.* **1991**, *335*, 377–392.
110. Thompson, R.N.; Morrison, M.A. Asthenospheric and lower-lithospheric mantle contributions to continental extensional magmatism: An example from the British Tertiary Province. *Chem. Geol.* **1988**, *68*, 1–15. [[CrossRef](#)]
111. Yilmaz, Y.; Polat, A. Geology and evolution of the Thrace volcanism, Turkey. *Acta Vulcanol.* **1998**, *10*, 293–303.
112. Coish, R.A.; Sinton, C.W. Geochemistry of mafic dikes in the Adirondack mountains: Implications for Late Proterozoic continental rifting. *Contrib. Miner. Petrol.* **1992**, *110*, 500–514. [[CrossRef](#)]
113. Cao, H.H. Geochronology and Geochemistry of the Late Paleozoic-Early Mesozoic Igneous Rocks in the Eastern Segment of the Northern Margin of the North China Block. Ph.D. Thesis, Jilin University, Changchun, China, 2013. (In Chinese with English Abstract)
114. Frey, F.A. Integrated models of basalt petrogenesis: A study of quartz tholeiites to olivine melilitites from south eastern Australia. *J. Petrol.* **1978**, *19*, 463–513. [[CrossRef](#)]
115. White, W.M.; Patchett, J. Hf-Nd-Sr isotopes and incompatible element abundances in island arcs: Implications for magma origins and crust-mantle evolution. *Earth Planet. Sci. Lett.* **1984**, *67*, 167–185. [[CrossRef](#)]
116. Polat, A.; Hofmann, A.W.; Rosing, M.T. Boninite-like volcanic rocks in the 3.7–3.8 Ga Isua greenstone belt, West Greenland: Geochemical evidence for intra-oceanic subduction zone processes in the early earth. *Chem. Geol.* **2002**, *184*, 231–254. [[CrossRef](#)]
117. Morrison, G.W. Characteristics and tectonic setting of the shoshonite rock association. *Lithos* **1980**, *13*, 97–108. [[CrossRef](#)]
118. Müller, D.; Rock, N.M.S.; Groves, D.I. Geochemical discrimination between shoshonitic and potassic volcanic rocks in different tectonic settings: A pilot study. *Miner. Petrol.* **1992**, *46*, 259–289. [[CrossRef](#)]
119. Foley, S.F.; Peccerillo, A. Potassic and ultrapotassic magmas and their origin. *Lithos* **1992**, *28*, 181–185. [[CrossRef](#)]
120. Turner, S.; Arnaud, N.; Liu, J.; Rogers, N.; Hawkesworth, C.; Harris, N.; Kelley, S.; Van Calsteren, P.; Deng, W. Post-collision, shoshonitic volcanism on the Tibetan plateau: Implications for convective thinning of the lithosphere and the source of ocean island basalts. *J. Petrol.* **1996**, *37*, 45–71. [[CrossRef](#)]
121. Williams, H.M.; Turner, S.P.; Pearce, J.A.; Kelley, S.P.; Harris, N.B.W. Nature of the source regions for post-collisional, potassic magmatism in southern and northern Tibet from geochemical variations and inverse trace element modelling. *J. Petrol.* **2004**, *45*, 555–607. [[CrossRef](#)]
122. McDonough, W.F.; Sun, S.S. The composition of the earth. *Chem. Geol.* **1995**, *120*, 223–253. [[CrossRef](#)]
123. Sajona, F.C.; Maury, R.C.; Bellon, H.; Cotton, J.; Defant, M.J.; Pubellie, M. Initiation of subduction and the generation of slab melts in western and eastern Mindanao, Philippines. *Geology* **1993**, *21*, 1007–1010. [[CrossRef](#)]
124. Elliott, T.; Plank, T.; Zindler, A.; White, W.; Bourdon, B. Element transport from slab to volcanic front at the Mariana arc. *J. Geophys. Res.* **1997**, *102*, 14991–15019. [[CrossRef](#)]
125. Klein, E.M.; Karsten, J.L. Ocean ridge basalt with convergent margin geochemical affinities from the Chile Ridge. *Nature* **1995**, *374*, 52–57. [[CrossRef](#)]
126. Hofmann, A.W.; Jochum, K.P.; Seufert, M.; White, W.M. Nb and Pb in oceanic basalts: New constraints on mantle evolution. *Earth Planet. Sci. Lett.* **1986**, *79*, 33–45. [[CrossRef](#)]
127. Saunders, A.D.; Storey, M.; Kent, R.W.; Norry, M.J. Consequences of plume-lithosphere interactions. In *Magmatism and the Causes of Continental Break-Up*; Geological Society, London, Special Publications; Storey, B.C., Alabaster, T., Pankhurst, R.J., Eds.; The Geological Society: London, UK, 1992; Volume 68, pp. 41–60.
128. Kieffer, B.; Arndt, N.; Lapierre, H.; Lapierre, H.; Bastien, F.; Bosch, D.; Pecher, A.; Yirgu, G.; Ayalew, D.; Eeis, D.; et al. Flood and shield basalts from Ethiopia: Magmas from the African superwell. *J. Petrol.* **2004**, *45*, 793–834. [[CrossRef](#)]

129. Wu, C.Z. Geochronology, geochemistry and tectonic significances of the Hongyuntan granitoids in the Qoltag area, eastern Tianshan. *Acta Petrol. Sin.* **2006**, *22*, 1121–1134, (In Chinese with English Abstract).
130. Zhang, Q.; Jiao, S.T.; Liu, H.Y. Significance of Sr and Yb to granite theory: Philosophical thinking on granite research. *Gansu Geol.* **2021**, *30*, 1–15, (In Chinese with English Abstract).
131. Ellam, R.M. Lithospheric thickness as a control on basalt geochemistry. *Geology* **1992**, *20*, 153–156. [[CrossRef](#)]
132. Xu, B.W.; Xi, A.H.; Ge, Y.H.; Liu, Y.; Wang, M.Z.; Fang, C. Zircon U-Pb ages of the Late Paleozoic A-type granites in Chifeng. *Acta Geol. Sin.* **2015**, *89*, 58–69, (In Chinese with English Abstract).
133. Huang, D.L.; Hou, Q.Y. Devonian alkaline magmatism in the northern North China Craton: Geochemistry, SHRIMP zircon U-Pb geochronology and Sr-Nd-Hf isotopes. *Geosci. Front.* **2017**, *8*, 171–181. [[CrossRef](#)]
134. Zhang, S.H.; Zhao, Y.; Song, B.; Liu, D.Y. Petrogenesis of the Middle Devonian Gushan diorite pluton on the northern margin of the North China block and its tectonic implications. *Geol. Mag.* **2007**, *144*, 553–568. [[CrossRef](#)]
135. Zhang, S.H.; Zhao, Y.; Liu, J.M.; Hu, J.M.; Song, B.; Liu, J.; Wu, H. Geochronology, geochemistry and tectonic setting of the Late Paleozoic-Early Mesozoic magmatism in the northern margin of the North China Block: A preliminary review. *Acta Petrol. Miner.* **2010**, *29*, 824–842, (In Chinese with English Abstract).
136. Niu, X.L.; Liu, F.; Feng, G.Y.; Mao, X.H. Petrogenesis of the Late Silurian to Early Devonian potassic alkaline rocks on the northern margin of the North China Craton and their constraints on the tectonic evolution. *Acta Petrol. Miner.* **2021**, *40*, 835–858, (In Chinese with English Abstract).
137. Liu, J.F.; Li, J.Y.; Chi, X.G.; Feng, Q.W.; Hu, Z.C.; Zhou, K. Early Devonian felsic volcanic rocks related to the arc-continent collision on the northern margin of North China Craton—Evidences of zircon U-Pb dating and geochemical characteristics. *Geol. Bull. China* **2013**, *32*, 267–278, (In Chinese with English Abstract).
138. Wang, H.C.; Xiang, Z.Q.; Zhao, F.Q.; Li, H.M.; Yuan, G.B.; Chu, H. The alkaline plutons in eastern part of Guyang County, Inner Mongolia: Geochronology, petrogenesis and tectonic implications. *Acta Petrol. Sin.* **2012**, *28*, 2843–2854. (In Chinese with English Abstract)
139. Defant, M.J.; Drummond, M.S. Derivation of some modern arc magmas by melting of young subducted lithosphere. *Nature* **1990**, *347*, 662–665. [[CrossRef](#)]
140. Pearce, J.A.; Harris, N.B.; Tindle, A.G. Trace element discrimination diagrams for the tectonic interpretation of granitic rocks. *J. Petrol.* **1984**, *25*, 956–983. [[CrossRef](#)]
141. Kinzler, R.J. Melting of mantle peridotite at pressures approaching the spinel to garnet transition: Application to mid-ocean ridge basalt petrogenesis. *J. Geophys. Res. Solid Earth* **1997**, *102*, 853–874. [[CrossRef](#)]
142. Walter, M.J. Melting of garnet peridotite and the origin of komatiite and depleted lithosphere. *J. Petrol.* **1998**, *39*, 29–60. [[CrossRef](#)]
143. Zhang, Y.P.; Su, Y.Z.; Li, J.C. Regional tectonics significance of the Late Silurian Xibiehe Formation in central Inner Mongolia, China. *Geol. Bull. China* **2010**, *29*, 1599–1605. (In Chinese with English Abstract)
144. Zhang, W.; Jian, P. SHRIMP dating of Early Paleozoic granites from north Damaoqi, Inner Mongolia. *Acta Geol. Sin.* **2008**, *82*, 778–787. (In Chinese with English Abstract)
145. Zhang, W.; Jian, P.; Kröner, A.; Shi, Y.R. Magmatic and metamorphic development of an Early to Mid-Paleozoic continental margin arc in the southernmost Central Asian Orogenic Belt, Inner Mongolia, China. *J. Asian Earth Sci.* **2013**, *72*, 63–74, (In Chinese with English Abstract). [[CrossRef](#)]
146. Shi, Y.R.; Liu, D.Y.; Miao, L.C.; Zhang, H.F.; Jian, P.; Zhang, W.; Hou, K.J.; Xu, J.Y. Devonian A-type granitic magmatism on the northern margin of the North China Craton: SHRIMP U-Pb zircon dating and Hf-isotopes of the Hongshan granite at Chifeng, Inner Mongolia, China. *Gondwana Res.* **2010**, *17*, 632–641. [[CrossRef](#)]
147. Sun, L.X.; Ren, B.F.; Teng, F.; Zhang, Y.; Gu, Y.C.; Guo, H. LA-ICP-MS zircon U-Pb ages of the volcanic rocks from the Chaotugou Formation in Aohan Banner, Inner Mongolia. *Geol. Bull. China* **2015**, *34*, 1493–1501. (In Chinese with English Abstract)
148. Wang, X.A. Tectonic Evolution in the Central Segment of the Northern Margin of the North China Plate from Early Paleozoic to Devonian. Ph.D. Thesis, Jilin University, Changchun, China, 2014. (In Chinese with English Abstract)
149. Chen, J.S.; Li, B.; Yang, H.; Liu, M.; Yang, F.; Li, W.; Wang, Y.; Cui, T.R. New zircon U-Pb age of granodiorite in Chifeng at the northern margin of North China Craton and constraints on plate tectonic evolution. *Acta Geol. Sin. (Engl. Ed.)* **2018**, *92*, 410–413. [[CrossRef](#)]
150. Wang, S.; Liang, H.J.; Wang, H.; Song, D.L.; Cheng, M.L.; Tan, C.L.; Ran, L.J.; Feng, Y.W.; Chen, Y.F.; Cui, Y.L.; et al. Discovery of the Late Devonian–Early Carboniferous bimodal volcanic rocks in the Aohanqi, Inner Mongolia and their geological significance. *Geochimica* **2020**, *49*, 150–167. (In Chinese with English Abstract)
151. Song, S.G.; Wang, M.M.; Xu, X.; Wang, C.; Niu, Y.L.; Allen, M.B.; Su, L. Ophiolites in the Xing’an-Inner Mongolia accretionary belt of the CAOB: Implications for two cycles of seafloor spreading and accretionary orogenic events. *Tectonics* **2015**, *34*, 2221–2248. [[CrossRef](#)]
152. Xie, W.; Song, X.Y.; Deng, Y.F.; Wang, Y.S.; Ba, D.H.; Zheng, W.Q.; Li, X.B. Geochemistry and petrogenetic implications of a Late Devonian mafic-ultramafic intrusion at the southern margin of the Central Asian Orogenic Belt. *Lithos* **2012**, *144–145*, 209–230. [[CrossRef](#)]

Disclaimer/Publisher’s Note: The statements, opinions and data contained in all publications are solely those of the individual author(s) and contributor(s) and not of MDPI and/or the editor(s). MDPI and/or the editor(s) disclaim responsibility for any injury to people or property resulting from any ideas, methods, instructions or products referred to in the content.